Computational and robotic modeling reveal parsimonious combinations of interactions between individuals in schooling fish

Liu Lei[1,2], Ramón Escobedo[2], Clément Sire[3], Guy Theraulaz[2,*]

1 University of Shanghai for Science and Technology, Shanghai, China
2 Centre de Recherches sur la Cognition Animale, Centre de Biologie Intégrative, Centre National de la Recherche Scientifique (CNRS), Université Paul Sabatier (UPS), Toulouse, France
3 Laboratoire de Physique Théorique, CNRS and UPS, Toulouse, France

* guy.theraulaz@univ-tlse3.fr

Abstract

Coordinated movements and collective decision-making in fish schools result from complex interactions by which individual integrate information about the behavior of their neighbors. However, little is known about how individuals integrate this information to take decisions and control their movements. Here, we combine experiments with computational and robotic approaches to investigate the impact of different strategies for a fish to interact with its neighbors on collective swimming in groups of rummy-nose tetra (*Hemigrammus rhodostomus*). By means of a data-based model describing the interactions between pairs of *H. rhodostomus* (Calovi *et al.*, 2018), we show that the simple addition of the pairwise interactions with two neighbors quantitatively reproduces the collective behaviors observed in groups of five fish. Increasing the number of neighbors with which a fish interacts does not significantly improve the simulation results. Remarkably, we found groups remain cohesive even when each fish only interacts with only one of its neighbors: the one that has the strongest contribution to its heading variation. But group cohesion is lost when each fish only interact with its nearest neighbor. We then investigated with a robotic platform the impact of the physical embodiment of the interaction rules and the combinations of pairwise interactions on collective motion in groups of robots. Like fish, robots experience strong physical constraints such as the need to control their speed to avoid collisions with obstacles or other robots. We find swarms of robots are able to reproduce the behavioral patterns observed in groups of five fish when each robot interacts only with the neighbor having the strongest effect on its heading variation, and increasing the number of interacting neighbors doesn't significantly improve the quality of group behavior. Overall, our results suggest that fish have to acquire only a minimal amount of information about their environment to coordinate their movements when swimming in groups.

Keywords: Collective behavior, Flocking, Fish school, Interaction networks, Computational modeling, Swarm robotics

Author Summary

How do fish combine and integrate information from multiple neighbors when swimming in a school? What is the minimum amount of information needed by fish about their environment to coordinate their motion? To answer these questions, we combine experiments with computational and robotic modeling to test several hypotheses about how individual fish could combine and integrate the information on the behavior of their neighbors when swimming in groups. Our research shows that, for both simulated agents and robots, using the information of two neighbors is sufficient to qualitatively reproduce the collective motion patterns observed in groups of fish. Remarkably, our results also show that it is possible to obtain group cohesion and coherent collective motion over long periods of time even when individuals only interact with their most influential neighbor, that is, the one that exerts the most important force on their heading variation.

Introduction

One of the most remarkable characteristics of group-living animals is their ability to display a wide range of complex collective behaviors and to collectively solve problems through the coordination of actions performed by the group members [1–3]. It is now well established that these collective behaviors are self-organized and mainly result from local interactions between individuals [4, 5]. Thus, to understand the mechanisms that govern collective animal behaviors, we need to decipher the interactions between individuals, to identify the information exchanged during these interactions and, finally, to characterize and quantify the effects of these interactions on the behavior of individuals [6,7]. There exists today a growing body of work that brought detailed information about the direct and indirect interactions involved in the collective behaviors of many animal groups, especially in social insects such as ants [8–11] and bees [12,13]. Recently, we introduced a new method to disentangle and reconstruct the pairwise interactions involved in the coordinated motion of animal groups such as fish schools, flocks of birds, and human crowds [14]. This method leads to explicit and concise models which are straightforward to implement numerically. It remains an open and challenging problem to understand how individuals traveling in groups combine the information coming from their neighbors to coordinate their own motion.

To answer this question, one first needs to know which of its neighbors an individual interacts with in a group, *i.e.*, who are the influential neighbors. For instance, does an individual always interact with its nearest neighbors, and how many? Most models of collective motion in animal groups have generally considered that each individual within a group was influenced by all the neighbors located within some spatial domain centered around this individual [15, 16]. This is the case in particular of the Aoki-Couzin model [17, 18] and the Vicsek model [19]. In the latter, each individual aligns its direction of motion with the average direction of all individuals that are located within a fixed distance in its neighborhood. Other models, more directly connected to biological data, consider that the interactions between individuals are topological and that the movement of each individual in the group only relies on a finite number of neighbors. This is the case in the works done on starling flocks [20, 21] and on barred flagtails (*Kuhlia mugil*) [22]. In golden shiners (*Notemigonus crysoleucas*), another work has sought to reconstruct the visual information available to each individual [23]. In this species, it has been shown that a model was best explaining the experimental data when all the neighboring individuals that occupy an angular area on the retina of a focal fish that is greater than a given threshold are taken into account. However, because of the cognitive load that is required for an individual to constantly monitor the movements of a large number of neighbors, it has been suggested that animals may focus their attention on a small subset of their neighbors [24–26]. In a previous work, we found experimental evidences that support this assumption. In groups of rummy nose tetras (*Hemigrammus rhodostomus*) performing collective U-turns, we found that, at any time, each fish pays attention to only a small subset of its neighbors, typically one or two, whose identity regularly changes [27]. However, we still ignore if the same pattern of interaction holds true when fish are schooling, *i.e.*, when individuals are moving together in a highly polarized manner and not performing some collective maneuver.

Then, one needs to know how does a fish integrate the information from its influential neighbors. The most common assumption is that animals respond by averaging pairwise responses to their neighbors (with added noise) [15–17]. However, existing work shows that the integration of information might be much more complex. In golden shiners, Katz *et al.* have shown that the combined effect of two neighbors on a fish response is close to averaging for turning, but somewhere between averaging and adding for speed adjustments [28]. This observation brings us back to a often neglected factor which is the impact of the physical constraints imposed on a fish movement by their body. Fish mainly achieve collision avoidance through the control of their speed and orientation at the individual level. However, existing models seldom treat collision avoidance in a physical way and most models assume that individuals move at a constant speed [6]. This is the main reason why these models cannot be directly implemented in real physical robotic systems [29].

To better understand how individuals combine and integrate interactions with their neighbors in a group of moving animals, we first analyze the dynamics of collective movements in groups of five *H. rhodostomus* moving freely in a circular tank. Then, we investigate different strategies for combining pairwise interactions between fish and analyze their impact on collective motion. To do that, we use the data-driven computational model developed by Calovi *et al.* [14] that describes the interactions involved in the coordination of burst-and-coast swimming in pairs of *H. rhodostomus*, and a swarm robotic platform that also allows us to investigate the impact of both direction and speed regulation. Finally, we compare the predictions of the computational and swarm robotics models with the experiments conducted under the same conditions with groups of fish. Our results show that individuals do not need to integrate the information about all their neighbors for a coordination to emerge at the group level. Indeed, if fish interact only with a single neighbor, the one having the strongest effect on the own heading variation, the group maintains its cohesion. Thus, each individual must interact with a very small number of neighbors, basically one or two, provided they are those who exert the stronger influence on its own movement.

Results

We collect three sets of data corresponding to i) our experiments with fish (*H. rhodostomus*), ii) our numerical simulations of the model derived in [14], and iii) our experiments with the robotic platform (see Fig. 1, S1 Video and S2 Video), from which we extract the trajectories of each individual (S3 Video). We characterize the collective behavior of fish, agents and robots by means of six quantities: the group cohesion $C(t)$, the group polarization $P(t)$, the mean distance to the wall of the tank $\langle r_{\rm w} \rangle (t)$, the relative orientation of the barycenter of the group with respect to the wall $\theta_{\rm w}^{B}(t)$, the index of rotation around the center of the tank $\Gamma(t)$, and the counter-milling index $Q(t)$, which measures the relative direction of rotation of individuals inside the group with respect to the direction of rotation of the group around the center of the tank (S4 Video). See Figs. 2 and 3 and the Material and Methods Section for the mathematical definition of these quantities.

We explore three different strategies of interaction between individuals and their neighbors with both the mathematical model and the swarm robotic platform. In the first strategy, individuals interact with their k nearest neighbors, with $k = 1$, 2 and 3. In the second strategy, the k neighbors are sampled randomly among the other $N - 1$

individuals, and in the third strategy, the k selected neighbors are those having the largest absolute contribution to the instantaneous variation of heading of the focal individual, as given by the model. We also study the cases where there is no interaction between individuals ($k = 0$) and the case where individuals interact with all the other individuals ($k = 4$).

We define the *influence of a neighbor on a focal individual* as the intensity of the contribution of this neighbor to the heading variation of the focal individual. This influence depends on the relative state of the neighbor with respect to the focal individual, which is determined by the triplet $(d_{ij}, \psi_{ij}, \phi_{ij})$, where d_{ij} is the distance between the focal individual i and its neighbor j, ψ_{ij} is the angle with which i perceives j, and ϕ_{ij} is the difference of the heading angles, a measure of the alignment between i and j (Fig. 2). The influence of j on the heading variation of i is estimated by means of the analytical interaction functions of the mathematical model derived in [14] for fish swimming in pairs, and defined in Eq. (7) in the Material and Methods section.

Collective behavior in fish experiments

Fish form cohesive groups with an average cohesion $C \approx 5$ cm (Fig. 4), they are highly polarized, with the 5 fish swimming in the same direction (huge peak at $P \approx 1$, Fig. 5), and remain quite close to the border of the tank, typically at $\langle r_{\rm w} \rangle \approx 7$ cm from the wall (Fig. 6), therefore almost always parallel to it (with a relative angle to the wall of the heading of the barycenter peaked at $\theta_{\rm w}^B \approx \pm\pi/2$, Fig. 7). Fish rotate clockwise (CW) or counter-clockwise (CCW) around the center of the tank (large peaks at $\Gamma \approx \pm 1$, Fig. 8).

Besides being the most frequently observed, these patterns take place mostly at the same time, as shown by the density maps of polarization with respect to cohesion (panels labeled "FISH" in S1 Fig–S4 Fig): groups are more cohesive when they are highly polarized, and have more or less the same cohesion for intermediate or low values of the polarization (although data become scarce for low values of P).

Quite frequently, groups are observed in which one fish swims in the opposite direction to that of the other four, as shown by the small bump at $P \approx 0.6$ in Fig. 5 and $\Gamma \approx \pm 0.6$ in Fig. 8. The contribution of a fish to the value of Γ is $+1$ when the fish rotates CCW and -1 when it rotates CW, in both cases perfectly parallel to the wall. Thus, the observed experimental values correspond to the case where $P = (1+1+1+1-1)/5 = 0.6$, and $\Gamma = (1+1+1+1-1)/5 = 0.6$ or $\Gamma = (-1-1-1-1+1)/5 = -0.6$. Less frequent, but still noticeable, are situations where two fish swim in the opposite direction to that of the other three, as shown by the slight bumps at $\Gamma \approx \pm 0.2$, corresponding to three fish swimming CW and the other two CCW (*i.e.*, $\Gamma \approx (-1-1-1+1+1)/5 = -0.2$) or, *vice versa*, three fish swimming CCW, and two CW ($\Gamma \approx (1+1+1-1-1)/5 = 0.2$).

In addition to the individual rotation of fish around the tank, measured by Γ, we also report a collective pattern consisting in individual fish rotating around the barycenter of the group in a direction which is precisely opposite to the direction of rotation of the group around the center of the tank (Fig. 3, S4 Video). We call this collective movement a *counter-milling behavior*, and define the instantaneous degree of counter-milling $Q(t)$ as a measure in $[-1, 1]$ of the intensity with which both rotation movements are in opposed directions: when $Q(t) < 0$, fish rotate around their barycenter B in the opposite direction to that of the group (*counter-milling*), while when $Q(t) > 0$, fish rotate mainly in the same direction around B than the group around T (*super-milling*).

Fig. 9 shows that fish exhibit a counter-milling behavior much more frequently than a super-milling behavior. Counter-milling behaviors result from the fact that fish located at the front of the group have to reduce their speed as they get closer to the border, due to their linear movement between two consecutive kicks. Fish located at the back of the group move faster and outrun the slowing down fish, relegating them to the back of the group. Then, the few fish at the front of the group approach the border, they slow down and are overtaken in turn by those who follow them. This maneuver is repeated successively, giving rise to the rotation of individual fish around the group center, in the opposite direction to the one that the group displays around the tank. This collective behavior resembles a perfectly coordinated swimming by relays which is nevertheless due to simple physical constraints, as already reported on wolf-packs hunting preys moving in circles [30].

Simulation results of the computational model

Collective motion in a circular tank

Panels (ABC) of Figs. 4–9 show the corresponding measures of the simulation data produced by the model for the different strategies of combination of the pairwise interactions. Panels (A) correspond to the strategy in which agents interact with the first nearest neighbors, panels (B) with neighbors chosen randomly, and panels (C) with neighbors selected according to the intensity of their influence on the focal agent. For the three strategies, we considered all the possible values of the number of neighbors with whom an agent interacts, $k = 1$, 2, 3, together with the case where there is no interaction between agents ($k = 0$) and the case where agents interact with every other agent ($k = 4$).

For comparison purposes, we have scaled the spatial axes of the PDFs corresponding to the model by a factor $\lambda_\mathrm{M} = 0.87$ (lines with different shades of blue in Figs. 4–9). This value is the minimizer of the l_1-norm of the difference between the PDF of group cohesion for fish data, and the PDF of group cohesion for the simulation data produced by the model when using the strategy involving the $k = 2$ most influential neighbors. As the x-axis is multiplied by λ_M, the y-axis of the PDF is divided by λ_M to preserve the normalized form having integral equal to 1. Noticeably, the fact that the value of λ_M is close to 1 indicates that the model produces a quite satisfactory quantitative approximation to the data of real fish.

When $k = 0$, no interaction exists between agents and, as expected, there is no formation of group: individuals turn around the tank, they are close and parallel to the wall, but remain scattered along the border ($C \approx 17.8\lambda_\mathrm{M}$ cm, $\langle r_\mathrm{w} \rangle \approx 15\lambda_\mathrm{M}$ cm), with a bell-shaped distribution of the polarization. Agents rotate around the tank in CW or CCW directions with the same probability, independently of the direction of rotation of the others; see the four huge peaks in the PDF of the rotation index (Fig. 8, gray lines) at $\Gamma = \pm 0.6$, corresponding to four agents turning in the same direction, and at $\Gamma = \pm 0.2$, where three agents turn in the same direction.

When $k = 1$, whatever the strategy used to select the neighbor (the nearest one, a random selected one or the most influential one), the measures immediately reveal that interactions are at play, with groups becoming cohesive ($C < 11\lambda_\mathrm{M}$ cm) and drastically closer to the wall ($\langle r_\mathrm{w} \rangle < 7\lambda_\mathrm{M}$ cm). Agents have frequently almost the same heading, the most often with 5 agents at the same time (clear peak at $P \approx 0.9$), but also in groups of 4 and 3 (slightly perceptible peaks at $P \approx 0.6$ and 0.2, respectively, in Fig. 5). Quite frequently also, the 5 agents have the same direction of rotation around the tank (large peaks at $\Gamma = \pm 1$), and situations where 4 or 3 agents have the same direction of rotation are frequent (peaks at $\Gamma = \pm 0.6$ and $\Gamma = \pm 0.2$ respectively, in Fig. 8).

For the three strategies, the measures on collective behavior are relatively far from those obtained in fish experiments. Interacting only with the nearest neighbor produces a much less compact group than interacting with the most influential neighbor (the PDF of $C(t)$ is much wider in Panel A than in Panel C in Fig. 4), while counter-milling practically doesn't exist when interacting with the nearest neighbor, but is already visible when interacting with the most influential one (S5 Fig). All strategies give rise to approximately the same level of polarization, while the rotation index is much more peaked at $\Gamma \approx \pm 1$ in the strategy that considers the nearest neighbor instead of the most influential one (Fig. 8A and C), although the central peaks are less pronounced in the PDF of the most influential strategy. The group is slightly closer to the border when individuals only interact with their nearest neighbor ($\langle r_{\rm w} \rangle$ is smaller and more peaked to the left in Panel A than in Panel C in Fig. 6). Note that when fish interact with a randomly chosen neighbor, group cohesion is worse than when they interact with the most influential one, but better than if they interact with their nearest neighbor (S5 Fig). Density maps show that one nearest neighbor is insufficient to convey the necessary information to reach the degree of cohesion and polarization observed in groups of fish (S1 Fig, S3 Fig).

When $k = 2$, all measures on collective behavior are improved, in the sense that they converge towards those observed in fish experiments. Whatever the strategy used to select the two neighbors, all individuals swim together and in the same direction, close to and along the border of the tank, and display a characteristic counter-milling behavior (S5 Fig). This is especially true for the distance to the wall, the rotation and counter-milling indices when fish interact with their nearest neighbors, whose measures overlap with those observed in real fish. Groups are indeed clearly more cohesive and more polarized than when using only one neighbor (Figs. 4–5). Cohesion and polarization coincide more frequently (S1 Fig, S3 Fig), and even more when neighbors are selected according to their influence. Even if quite satisfactory when compared to fish, other measures when interacting with two influential neighbors are not better than when interacting with the two nearest ones; see, *e.g.*, counter-milling (Fig. 9).

As noted previously, when fish interact with two neighbors randomly chosen, the characteristics of collective movements are intermediate between those obtained with the other two strategies. In particular, the results are better than those obtained with the strategy based on spatial proximity, due to the fact that at least one neighbor is shared 5/6 of the time, and both neighbors are the same in 1/6 of the time. Note also that it may happen that one of the two nearest neighbors may be located behind the focal fish, so that its influence on the focal fish is negligible with respect to the influence of the other neighbor, a situation that amounts for the focal fish to interact with only one neighbor.

When interacting with $k = 3$ neighbors, results are almost identical for the three strategies because neighbors are the same a high percentage of the time (25% of the time the selected neighbors are the same, 75% of the time there are at least 2 neighbors in common to all the strategies, and there is always at least one neighbor in common). Using the 3 nearest neighbors instead of 2 only improves group cohesion, while using the 3 most influential ones, instead of 2, doesn't improve any of the measures, including density maps (S1 Fig, S3 Fig), and is even worse for counter-milling (Fig. 9, S5 Fig).

Using the $k = 4$ neighbors to interact with doesn't improve the cohesion and polarization of the group in comparison to the preceding condition when $k = 3$.

Collective motion in an unbounded space

The model allows us to simulate a condition where agents are swimming in an unbounded space by removing the interaction with the wall. This condition is particularly important to study in order to measure the impact of the confinement of agents by the arena on group cohesion.

Fig. 10 shows the time evolution of group cohesion for the strategies of paying attention to the k most influential neighbors or to the k nearest neighbors, for $k = 1$ to 4. Despite the fact that the wall is no longer present to keep the agents together, all the strategies except the one that consists in interacting only with the nearest neighbor allow the group to remain cohesive for more than 2.5 hours ($\approx 10^4$ kicks) in numerical simulations (Fig. 10ABC). Note that when fish only interact with the most influential neighbor, the group is highly cohesive ($\lambda_M C(t) \approx 0.1$ m, Fig. 10A), but less than in the arena ($\lambda_M C(t) \approx 0.07$ m, Fig. 4). This shows that the arena reinforces the cohesion of the group. However, when fish interact only with their first nearest neighbor the group disintegrates very quickly and then diffuses, with $C^2(t)$ growing linearly in time (Fig. 10C). In any case, the strategies that consist in interacting with the most influential neighbors always lead to more cohesive groups than when agents interact with the nearest ones. In addition, the choice of neighbors with which the agents interact also determines the distance d_{cut} beyond which an agent no longer perceives the attraction exerted by another agent.

When the attraction range between agents decreases, the model shows that for a fixed duration of the simulation, there exists a critical distance d^*_{cut} beyond which the agents do not interact anymore and freely diffuse until the end of the simulation (Fig. 10DE). The value d^*_{cut} depends on the strategy of interaction between agents. When the agents only interact with their most influential neighbor, the critical distance is $d^*_{\text{cut}} \approx 0.9$ m, and is slightly shorter for $k = 2$, 3 and 4 (around 0.75 m, Fig. 10D), while when the agents interact with the nearest neighbors, d^*_{cut} is around the same value than for the previous strategy when $k = 3$, but it is quite higher for $k = 2$ (around 3.5 m), and even doesn't exist when $k = 1$. In that case, whatever the value of d_{cut}, the intensity of the attraction is not strong enough to keep the group cohesive (see the plateau for $d_{\text{cut}} \geq 1$ m in Fig. 10E).

Collective behavior in swarm robotics experiments

Panels (DEF) of Figs. 4–9 show the results of the robotic experiments performed in the same conditions as those studied with the model, including the case where robots do not interact with each other and the case where each robot interacts with all the others. Counter-milling in robots is shown in S6 Fig, and the density maps of cohesion and polarization are shown in S2 Fig and S4 Fig. The robotic platform and the monitoring of a swarm of 5 robots in motion are shown in S2 Video.

In general, the results of the robotic experiments are qualitatively very similar to those found in the simulations of the model, despite the physical constraints of real world. The main difference with the model concerns the control of speed by the robots to avoid collisions with the circular wall and other robots. This difference is especially relevant when $k = 0$ because, in the model, agents are point particles and behave exactly as if they were alone in the arena.

Despite the fact that the size of the robotic platform has been scaled to correspond to that of the set-up used in the experiments with fish, the border has a stronger effect on the robots. Indeed, the collision avoidance protocol induces effective interactions between the robots that have a longer range than the interactions between fish. We found a much smaller scaling factor than in model simulations: $\lambda_{\text{R}} = 0.35$.

When $k = 0$, robots move independently from each other when they are sufficiently far from each other, and tend to remain dispersed along the border of the arena (S5 Video): the group cohesion is weak ($C \approx 10\lambda_{\text{R}} = 28.5$ cm), and the mean distance to the wall is large ($\langle r_{\text{w}} \rangle \approx 10\lambda_{\text{R}}$ cm). Robots are relatively more cohesive and closer to the wall than simulated agents because the confining effects of the border of the arena are stronger in robots than in agents (see Figs. 4, 6, S2 Fig and S6 Fig). Robots are mainly not polarized and exhibit the same peaks in the rotation index as those observed in the simulations for the same condition $k = 0$. The peaks observed in the PDF of the robots (Fig. 8D) are however much smaller than those of the model (Panel A, same figure); this is due to the fact that when two robots meet, the collision avoidance procedure forces them to change direction, thus breaking the continuity of their walk along the border, in opposition to what occurs in the model, since the point particles do not avoid each other when $k = 0$.

Interacting only with $k = 1$ nearest neighbor does not allow robots to coordinate their motion and move as a coherent group (see S6 Video). Panel (D) of Figs. 4–9 show that the curves almost overlap with those obtained for $k = 0$, see, *e.g.*, the cohesion, the polarization, the mean distance to the wall, and the counter-milling, which is not visible (S6 Fig). On the other hand, when the robots interact with their most influential neighbor (S7 Video), the group is highly cohesive ($C(t) < 6.5\lambda_{\rm R} = 17$ cm, compared to $10\lambda_{\rm R} = 28.5$ cm when interacting with the nearest neighbor), highly polarized (large peak at $P = 1$, while there is no peak at all when interacting with the nearest neighbor), and individuals move quite close to the border ($\langle r_{\rm w}\rangle \approx 7\lambda_{\rm R} = 20$ cm, instead of $10\lambda_{\rm R} = 28.5$ cm). Counter-milling is clearly visible (S7 Video and S6 Fig), and the similarity of the density maps of cohesion and polarization with those found in fish is the highest (S2 Fig and S4 Fig). Note that the rotation index doesn't display the two high peaks at $\Gamma = \pm 1$. This is due to the fact that the width of the group is frequently quite large (> 18 cm) with respect to the size of the arena ($R = 42$ cm). Thus, when the group of 5 robots moves slightly towards the center of the arena ($r_{\rm w} > 25$ cm from the border), one robot can end up on the other side of the arena with respect to its center When this happens, the contribution of this robot to the rotation index is opposite to the one of the other four, thus reducing the value of Γ, although the group is in perfect rotation around the tank.

Finally, for the strategy consisting in picking $k = 1$ neighbor randomly, the results are somewhat intermediate between those for the nearest and the most influential neighbor strategies, in terms of polarization, cohesiveness, rotation, and counter-milling (S8 Video). This intermediate features are in fact typical of this random strategy, as already observed in the model.

Extending the interaction with the $k = 2$ nearest neighbors reinforces the coordination and coherence of the group (S9 Video), which is more cohesive, $C(t)$ decreases from around $10\lambda_{\rm R} = 28.6$ cm to $7\lambda_{\rm R} = 20$ cm, and simultaneously more frequently polarized (S2 Fig), although polarization is still small: the PDF has a wide region of high values centered in $P \approx 0.85$, and is not peaked at $P = 1$. The high peak at $P = 0.6$ reveals that situations in which groups of 4 robots move in the same direction while the fifth one moves in the opposite direction are quite frequent (Fig. 5D). Wide groups (larger than 18 cm, Fig. 4D) moving far from the border (more than 22 cm, Fig. 6D) are still frequent, and counter-milling is not yet visible (S6 Fig). On the contrary, interacting with a second influential neighbor definitively produces patterns that are similar to those observed in fish experiments, especially if we consider the polarization, where the peak at $P = 1$ clearly narrows and doubles its height (S10 Video and Fig. 5F), although the improvement with respect to the strategy that consists in interacting only with the most influential neighbor is small, or even negligible, if we consider the counter-milling index (Fig. 9). Regarding the rotation index, interacting with 2 most influential neighbors instead of one degrades the result: the central region of the PDF is higher and the peaks at $\Gamma = \pm 1$ disappear (Fig. 8F), due to the same phenomenon described above, when the group is effectively rotating around the center of the arena but one or two robots cross to the other side of the arena.

Again, the strategy consisting in picking $k = 2$ random neighbors leads to results markedly better than the $k = 2$ nearest neighbors strategy, and almost similar to the $k = 2$ most influential neighbors strategy, in terms of polarization, cohesiveness, rotation, and counter-milling (see S11 Video).

One can improve the results only when the robots interact with a third neighbor ($k = 3$) and whatever the interaction strategy which is considered. In that case, all strategies always share at least 2 neighbors (see S12 Video and S13 Video). Indeed, when $k = 3$, the PDF of the polarization displays the huge peak at $P = 1$ observed in groups of fish (including the bump at $P = 0.6$, Figs. 5DE), the group is more cohesive

(C decreases to a mean value of $6\lambda_{\mathrm{R}} = 17$ cm and has a quite narrow PDF, Fig. 4DE) and polarized at the same time (S2 Fig), robots remain at a mean distance from the border of less than $6\lambda_{\mathrm{R}}$ cm, with also a narrow PDF similar to the one found in our fish experiments (Fig. 6DE), and counter-milling is clearly visible (S6 Fig). The results corresponding to the strategy that consists for a robot in interacting with its $k = 3$ most influential neighbors are omitted because they are statistically indistinguishable from those obtained when $k = 2$.

As we already observed in model simulations, the strategy that consists in interacting with neighbors randomly chosen leads to collective movements whose characteristics are intermediate between those obtained with the other two strategies (S13 Video). In particular, the results are closer to those observed in experiments with fish than those obtained when the robots interact with their nearest neighbors.

When robots interact with $k = 4$ neighbors (S14 Video), the cohesion, the mean distance to the wall and the counter-milling are not improved in comparison to the condition when interacting with the $k = 3$ nearest or random neighbors. Results are also quite similar to the condition when robots interact with the 2 most influential ones (Figs. 4, 6 and 9), while the group exhibits a higher peak at $P = 0.6$ (Fig. 5) and the rotation index is almost flat (Fig. 8).

Discussion

Collective motion involving the coherent movements of groups of individuals is primarily a coordination problem. Each individual within a group must precisely adjust its behavior to that of its neighbors in order to produce coordinated motion. Previous works have suggested that, instead of averaging the contributions of a large number of neighbors, as suggested by many models [17–19, 22], individuals could pay attention to only a small number of neighbors [24–27]. This mechanism would overcome the natural limitation of amount of information each individual can handle [31]. Determining how these relevant neighbors are chosen at the individual scale is therefore a key element to understand the coordination mechanisms in moving animal groups.

Here, we addressed this question in groups of *H. rhodostomus* swimming in a circular tank. This species of fish is of particular interest because of its tendency to form highly polarized groups and its burst-and-coast swimming mode [14], which allows us to consider that each fish adjusts its heading direction at the onset of each bursting phase, that is labeled as a “kick”. Just before these brief accelerations, the fish integrates the information coming from its environment and performs the kick in the right direction.

In our experiments, groups of 5 fish remain highly cohesive, almost perfectly polarized, and turn around the tank in the same direction for very long periods while remaining close to the wall. Individual fish are also able to occasionally reverse their direction of motion with respect to those of other fish, and display a remarkable counter-milling collective behavior consisting in individual fish rotating around the group barycenter in the opposite direction to that of the group in the tank, so that individuals alternate their positions at the front of the group.

Based on a previous work in which we have reconstructed and modeled the form of the interactions of *H. rhodostomus* fish swimming in pairs [14], we analyzed three strategies of combining the pairwise interactions between a focal fish and a number $k = 1$ to 3 of its neighbors by means of a computational model and a robotic platform. In the first strategy, neighbors were selected according to their distance to the focal individual. In the second strategy, neighbors were randomly chosen, and in the third strategy, neighbors were selected according to the intensity of their contribution to the heading variation of the focal individual. The impact of these strategies on the resulting collective behavior was then measured and analyzed by mean of six quantities: group cohesion, polarization index, rotation index, mean distance and relative orientation of the barycenter with respect to the border of the tank, and counter-milling index.

Our results suggest that when individuals (agents or robots) interact with a minimal number of neighbors, namely two, a group of individuals is able to reproduce the main characteristics of the collective movements observed in the fish experiments. Remarkably, our results also show that it is possible to obtain coherent collective motion even when individuals only interact with their most influential neighbor, that is, the one that exerts the most important force on their heading variation. Moreover, when individuals interact with k randomly selected neighbors, the results are closer to the ones observed in fish experiments than when they interact with their k nearest neighbors.

In the simulations of the model, when the agents are interacting with a single neighbor, this immediately leads to the formation of groups. Whatever the strategy used to select a neighbor (the nearest one, a randomly chosen one or the most influential one), the quantities used to quantify group behavior show that the exchange of information with a single neighbor leads agents to get closer to each other at least temporarily. However, whatever the strategy considered, cohesion, polarization and milling are still weak, suggesting that agents often remain alone and move independently. The simulations of the model in an open-bounded space show that group cohesion is maintained over long periods of time when agents only interact with their most influential neighbor, provided the attraction range is above a critical threshold distance. However, when agents only interact with their nearest neighbor, this automatically leads to the dispersion of the group, which diffuses at a constant rate. Therefore, the cohesion of the group observed in the arena is not a consequence of the confinement of the agents, but mainly results from the higher quality of the information provided by the influential neighbors in comparison to the one provided by the nearest neighbors.

Then, when agents acquire more information about their environment (*i.e.*, when $k = 2$), all the interaction strategies implemented in the model give rise to collective behaviors that are in qualitative agreement with those observed in the experiments with fish, and a quantitative agreement is even reached for some quantities characterizing group behavior. But interaction strategies do not have the same effect on group behaviors: when agents interact with their most influential neighbors instead of the nearest ones, the cohesion is stronger, groups are more polarized, individuals reverse less, and milling is more frequent. When agents collect even more information about their environment (*i.e.*, when they pay attention to $k = 3$ neighbors), the agreement with fish experiments is not improved if the neighbors are chosen according to their influence; however, groups become more cohesive and polarized when the agents interact with their nearest neighbors. Note that when agents interact with three neighbors, distinguishing the effects of the different interaction strategies becomes difficult since all agents always share at least two neighbors. Interacting with randomly chosen neighbors gives rise to group behaviors whose characteristics are intermediate between those resulting from the other two strategies, since when the agents are doing a random choice, they frequently select one or the other nearest or most influential neighbors. In summary, the simulation results clearly indicate that group behaviors similar to those observed in fish experiments can be reproduced by our model, provided that individuals interact with at least two of their neighbors at each decision time. In turn, no clear gain is obtained when agents interact with a third additional neighbor when the agents use a strategy based on influence, while group cohesion is only slightly improved when the agents use a strategy based on distance.

By implementing the behavioral fish model and the same local interaction strategies in our robotic platform, we also investigate the impact of the physical constraints and the collision avoidance protocols based on speed control on the group behavior. As in the model simulations, the strategy based on the influence exerted by the neighbors on the instantaneous direction change is much more efficient than the strategy based on the distance of the neighbors to the focal robot. Remarkably, and as already observed in the model simulations, when robots only interact with their most influential neighbor, the group remains permanently cohesive, close to the border and highly polarized. Moreover, in that condition, robot reversions rarely occur, at least not as frequently than in groups of fish. By contrast, when robots only interact with their nearest neighbor, they are not able to exhibit any kind of coordinated behavior. Everything happens as if pairwise interactions between robots were masked by the effect induced by the collision avoidance protocols: the group cohesion, the polarization, and the mean distance of the group to the border are almost identical to those obtained with the null model, in which no interaction exists between robots except collision avoidance. When robots interact with two neighbors, the agreement with the results of fish experiments is improved, but it is only when robots interact with three neighbors that the strategy based on the distance produces highly cohesive and polarized groups that move close to the border and that rotate in a counter-milling way around the arena.

Overall, our results show that each individual must acquire a minimal amount of information about the behavior of its neighbors for coordination to emerge at the group level. This property could serve as a support for selective attention mechanisms, thus allowing individuals to adapt to information overload when they move in large groups [31].

Materials and Methods

Experimental procedures and data collection

Ethics statement. Our experiments have been approved by the Ethics Committee for Animal Experimentation of the Toulouse Research Federation in Biology N° 1 and comply with the European legislation for animal welfare.

Study species. Rummy-nose tetras (*Hemigrammus rhodostomus*) were purchased from Amazonie Labège (http://www.amazonie.com) in Toulouse, France. Fish were kept in 150 L aquariums on a 12:12 hour, dark:light photoperiod, at 25.2 °C (±0.7 °C) and were fed *ad libitum* with fish flakes. The average body length of the fish used in these experiments is 31 mm (±2.5 mm).

Experimental setup. We used a rectangular experimental tank of size 120×120 cm, made of glass, that we set on top of a box to isolate fish from vibrations. The setup was placed in a chamber made by four opaque white curtains surrounded by four LED light panels to provide an isotropic lighting. A circular tank of radius $R = 250$ mm was set inside the experimental tank filled with 7 cm of water of controlled quality (50% of water purified by reverse osmosis and 50% of water treated by activated carbon) heated at 24.9 °C (±0.8 °C). Reflections of light due to the bottom of the experimental tank are avoided thanks to a white PVC layer. Each trial started by setting groups of fish randomly sampled from the breeding tank into the circular tank. Fish were let for 10 minutes to habituate before the start of the trial. A trial consisted in one hour of fish freely swimming (*i.e.*, without any external perturbation) in the circular tank. Fish trajectories were recorded by a Sony HandyCam HD camera filming from above the setup at 25 Hz (25 frames per second) in HDTV resolution (1920×1080p). We performed 11 trials with groups of $N = 5$ fish.

Swarm robotic platform

Robots. We used a swarm robotic platform composed by small compact mobile robots that we called "Cuboids", a name chosen in reference to the first realistic computer program that simulated the flocking behavior in birds and the schooling behavior in fish, called "Boids", developed in 1986 by Craig Reynolds [32]. The Cuboids robots were specifically designed by us for this experiment.

Cuboids have a square basis of 40 mm×40 mm, they are 60 m high and weigh 50 grams (Fig. 11). We now describe the elements of a Cuboid; numbers between parentheses refer to labels in Fig. 11. Each robot is equipped with two differential wheels (7) driven by small DC motors (13). The small belts (9) connect wheels to the DC motors, which can drive the robot with a maximum speed of 50 mm/s. The two wheels are mounted on a central axis (6). An IEEE 802.11n/WIFI module (8) with a range of approximately 200 meters is used for communication network between robot and a wireless router. A Li-Poly rechargeable battery (15) provided energy for about 6 hours in our experimental conditions. In addition, a coil (12) located under the robot, can be used to charge the robot wirelessly while it is working. The charging circuit is located on the side board (11). The robot bottom hosts a 32-bit, 168 MHz ARM microprocessor STM32F4 (14), which can provide multi control loops with the time duration up to 2ms. Besides, another 8-bit microcontroller PIC18F25k22 is mounted on the top sensor board (1), which controls a LCD screen (16) to display information and a 3-colors LED (17). The microprocessor communicates with the microcontroller by 4 copper bars (4), which can simultaneously provide power and communication bus.

Each Cuboid also has several sensors to measure the relative positions of other robots in its neighborhood and to send and receive messages from these robots. Within a sensing range of about 20 cm, a robot can send messages infrared signals by the center IR transmitter (3). There are two IR receivers (2) on both sides of the robots, which can determine the distance of a neighboring robot that transmit the infrared signal. From the two distance values provided by the IR receivers, the peering angle of this neighboring robot can be calculated by triangulation method. Furthermore, the relative position of the neighboring robot to the focal one can be computed by the information of distance and peering angle acquired before. On the other side, the IR signal also carries a short message that includes information on robot ID, orientation angle, speed and states. Moreover, each robot keeps a list of its neighbors with this information that is updated with time. If the robot does not receive the IR signal transmitted by a neighbor who is already in the list for a long time, the item related to this neighbor is deleted from the list. The heading of a Cuboid is measured by a motion tracking sensor MPU-9250 (18). This device consists of a 3-Axis gyroscope, a 3-Axis accelerometer and 3-Axis magnetometer. Hence, the MPU-9250 is a 9-axis Motion Tracking device that also combines a Digital Motion Processor. With its I2C bus connected with PIC18F25K22, the MPU-9250 can directly provide complete 9-axis Motion Fusion output to the microcontroller. These sensing and local communication devices have not been used in the experiments that have been done in a supervised mode.

Experimental platform. The robotic experimental setup consisted of a circular arena of radius 420 mm resting on a 1 m×1 m square flat surface with a camera (Basler piA2400-17gc) mounted on the top (see Fig. 12). A computer is connected to the camera to supervise the actions performed by the robots in the arena, and to perform the necessary image processing to track each robot and compute in real time its position (x, y) and heading angle ϕ.

The loop cycle of the imaging process module is 300 ms, a limit imposed by camera's updating speed. A tracking software (Robots ID Tracker) based on the Kalman filter technology, is then used to assign the location data to the right robots on a shorter time scale (every 20 ms). These data are used in real time to control the reaction of each robot in its changing environment, and are also stored in the computer for off-line *a posteriori* trajectory analysis. Thanks to the high precision of our tracking system, we are able to compute in real time and for each robot the quantities that characterize their instantaneous state with respect to their environment: the distance and relative orientation to the wall r_w and θ_w, and the distance, relative angular position and relative orientation with respect to each neighbor, d_{ij}, ψ_{ij} and ϕ_{ij}, respectively (Fig. 2). All this information is used to compute the output of the interactions of a robot with its local environment by means of an Object-Oriented Programming software developed by us. Then, we compute the result of the mathematical model that controls the robot behavior, which combines the interactions with the obstacles and with the other robots, and generates the control signals dispatched in a distributed way to each individual robot through a WIFI communication router (HUAWEI WS831).

Fig. 13 shows the "hardware in loop" (HIL) simulation used to control the Cuboids robots. Each robot includes three fundamental parts: the sensors used to detect the local environment, a processor for computing its decisions, and the actuators to carry out the displacement. Although the robots are perfectly autonomous and can perform all the data collection and processing on-board, programming a robot is a time demanding task that must be repeated for each new experimental condition, so that, taking profit of the high speed communication system we implemented, we decided to execute the decision-making on the external computer, taking care of mimicking the conditions of autonomy and decentralization of the system. The HIL simulation integrates the robots hardware into the distributed control loops of the platform computer software. As such, it differs from a traditional software simulation, being a *semi-real* one. Compared with pure theoretical simulations "in silico", the HIL simulation integrates the hardware constraints and provides more practical results in the physical environment.

Data extraction and pre-processing

Fish data were extracted from videos recorded during 11 sessions along 11 days in 2013, by means of idTracker software version 2.1 [33], producing 11 data files with the position (in pixels) of each fish in each frame, with a time step of $\Delta t = 0.04$ s (corresponding to images taken with a frequency of 25 fps). Data were located in a rectangle of size $[471.23, 1478.48] \times [47.949, 1002.68]$ containing the circular tank of diameter 50 cm. The conversion factor from pixels to meters is 0.53×10^{-3} m/pix. The origin of coordinates $T(0,0)$ is set to the center of the tank (Fig. 1).

We found that trajectory tracking was satisfactorily accurate. However, fish were often misidentified, making impossible the direct use of the data provided by the tracking system. We thus implemented a procedure of identity reassignment that provided us with the proper individual trajectories. In short, the procedure is a kind of bubble sort algorithm where fish identities are successively reassigned in such a way that the coordinates of each fish at the next time step are the closest ones to the coordinates they had at the previous time. That is, the fish i at time t is assigned the coordinates of fish j at time $t + \Delta t$ that minimize the distance covered by the 5 fish.

Data were then grouped in a single file, counting 1.077.300 times, *i.e.*, almost 12 hours where the position of each fish is known. Then, times where at least one fish freezes were removed. Fish often remain stationary. We considered that a fish is at rest when the distance covered in 60 frames is smaller than 30 pixels, that is, when the mean speed is smaller than 6.6 mm/s during at least 2.4 seconds. We erased more than half of the data (around 5h 30mn remained). We then extracted the continuous sequences lasting at least 20 seconds, obtaining 293 sequences for a total duration of around 3h 10mn. This provided us with almost 16 hours of observation of single fish trajectories, as there are 5 fish, and their kicks are asynchronous.

Fish trajectories were then segmented according to the burst-and-coast typical behavior of this species [14]. We used a time window of 0.2 s to find the local maxima of the velocity. These points are used to define the onset of a kick event. We detected 60312 kicks, which means that a fish makes in average around 1 kick/s.

For statistical purposes, we assumed that, for a given trajectory, its symmetric trajectory with respect to the horizontal line has the same probability of occurrence [14]. This allowed us to double our data set by adding the symmetric trajectories, thus reducing the statistical uncertainty on quantities depending on angles (by a factor $\sqrt{2}$). Note that, in the symmetric trajectory, the y-coordinate and all the angles have the opposite sign with respect to the original trajectory. Counting also the symmetric trajectories, we sum up to 120624 equiprobable kicks.

To calculate the heading angle of a fish at time t, we considered that the direction of motion is well approximated by the velocity vector of the fish at that time t. The heading angle $\phi(t)$ is thus given by the angle that its velocity vector $\vec{v} = (v_x, v_y)$ makes with the horizontal line, that is,

$$\phi(t) = \mathtt{ATAN2}\left(v_y(t), v_x(t)\right). \tag{1}$$

Positive angles are measured in counter-clockwise direction and `ATAN2` returns a value in $(-\pi, \pi]$. The components of the velocity are estimated with backward finite differences, *i.e.*, $v_x(t) = (x(t) - x(t - \Delta t))/\Delta t$ and $v_y(t) = (y(t) - y(t - \Delta t))/\Delta t$.

The robots' trajectories were extracted with a custom-made tracking software based on Kalman filter and pattern recognition technology [34]. Data were recorded every $\Delta t = 0.04$ s, and trajectories were then subjected to the same treatment.

Computational model

Hemigrammus rhodostomus performs a "burst-and-coast" swimming behavior characterized by sequences of sudden speed increases called "kicks" followed by quasi-passive, straight decelerations (S1 Video, S3 Video). The decisions of fish to change their heading are considered to occur exactly at the onset of the accelerations [14]. To reach some place, a fish changes its direction of motion while accelerating at the same time, and then slides almost straight towards the target place. Here we use the same model to control the decisions of fish in simulation and the decisions of robots.

The new vector position $\vec{u}_i^{n+1}$ of an agent i (fish or robot) at time step $n+1$ is determined by the following discrete decision model:

$$\vec{u}_i^{n+1} = \vec{u}_i^{n} + l_i^n \, \vec{e}\,(\phi_i^{n+1}), \tag{2}$$

$$\phi_i^{n+1} = \phi_i^n + \delta\phi_i^n, \tag{3}$$

where l_i^n is the kick length of this agent at time step $n+1$, $\vec{e}\,(\phi_i^{n+1})$ is the unitary vector pointing in the direction of angle ϕ_i^{n+1}, and $\delta\phi_i^n$ is the heading variation of the agent at time step $n+1$, resulting from the *decision process* of the agent (Fig. 1C).

Two parameters have to be computed to determine a new target place: the kick length l_i^n and the variation of the heading angle $\delta\phi_i^n$. The kick length is sampled from the bell-shaped distribution of kick lengths obtained in our experiments of fish swimming in pairs [14], whose mean value is $l = 7$ cm. When the new computed position of the agent would be outside of the tank, a new kick length is sampled from the distribution. The typical velocity of fish in their active periods was found to be $\mathrm{v}_0 = 14$ cm/s, decaying exponentially during kicks with a relaxation time $\tau_0 = 0.8$ s. The duration of the time step $n+1$ is thus determined by the length of the kick and the speed of the fish [14].

The variation of the heading angle from one time step to another is considered to be the sum of the variations induced by the environment of the agent, that is,

$$\delta\phi_i^n = \delta\phi_{\mathrm{w},i}^n + \delta\phi_{\mathrm{R},i}^n + \sum_{j=1, j\neq i}^{N} \delta\phi_{ij}^n, \tag{4}$$

where $\delta\phi_{\mathrm{w},i}^n$ is the angular variation caused by static obstacles (the wall of the fish tank or the border of the robot platform), $\delta\phi_{\mathrm{R},i}^n$ is a Gaussian white noise included in the spontaneous decision of the fish to change its heading, and $\delta\phi_{i,j}^n$ is the angular variation induced by the social interaction of the focal agent i with its neighbor j.

Each contribution to the angle variation can be expressed in terms of decoupled functions of the instantaneous state of the agents, that is, the distance and relative orientation to the wall r_w and θ_w, and the distance and relative orientation and alignment with neighbors, d, ψ and ϕ, respectively (Fig. 2A). The derivation of these functions is based on physical principles of symmetry of the angular functions and a sophisticated procedure detailed in Calovi *et al.* [14].

For completeness, we show these functions in S7 Fig and present here their analytical expressions with the parameter values necessary to reproduce the simulations.

- The repulsive effect of the wall is a centripetal force that depends only on the distance to the wall r_w and the relative angle of heading to the wall θ_w. Assuming that this dependence is decoupled, *i.e.*, $\delta\phi_\mathrm{w}(r_\mathrm{w}, \theta_\mathrm{w}) = F_\mathrm{w}(r_\mathrm{w})\, O_\mathrm{w}(\theta_\mathrm{w})$, we have:

$$F_\mathrm{w}(r_\mathrm{w}) = \gamma_\mathrm{w} \exp\left[-\left(\frac{r_\mathrm{w}}{l_\mathrm{w}}\right)^2\right], \quad O_\mathrm{w}(\theta_\mathrm{w}) = \beta_\mathrm{w} \sin(\theta_\mathrm{w})\Big(1 + 0.7\cos(2\theta_\mathrm{w})\Big), \tag{5}$$

  where $\gamma_\mathrm{w} = 0.15$ is the intensity of the force ($F_\mathrm{w}(0) = \gamma_\mathrm{w}$), $l_\mathrm{w} = 0.06$ m is the range of action, and $\beta_\mathrm{w} = 1.9157$ is the normalization constant of the angular function $O_\mathrm{w}(\theta_\mathrm{w})$, so that the mean of the squared function in $[-\pi, \pi]$ is equal to 1, that is, $(1/2\pi)\int_{-\pi}^{\pi} O_\mathrm{w}^2(\theta)d\theta = 1$. All angular functions are normalized like that to simplify the direct comparison of their shape in the different interactions.

  These parameter values are those used in the model simulations. They also appear in Table 1, together with the values used in the experiments with robots.

- The random variation of heading $\delta\phi_\mathrm{R}$ depends on the distance to the wall r_w, as the interaction with the wall dominates the random heading variation when the individual is close to the wall. Thus, we write

$$\delta\phi_\mathrm{R}(r_\mathrm{w}) = \gamma_\mathrm{R}\left(1 - \alpha \exp\left[-\left(\frac{r_\mathrm{w}}{l_\mathrm{w}}\right)^2\right]\right) g, \tag{6}$$

  where $\gamma_\mathrm{R} = 0.45$, $\alpha = 2/3$, and g is a random number sampled from a normal distribution (0 mean, 1 st. dev.). Random variations are minimal at the border, where $r_\mathrm{w} = 0$, $\delta\phi_\mathrm{R} = \gamma_\mathrm{R}(1-\alpha)g$, and become larger as the individual moves away from the border, *i.e.*, as r_w grows. Far from the border, the exponential goes to zero and $\delta\phi_\mathrm{R} = \gamma_\mathrm{R} g$.

- We assume that the interaction between agents can be decomposed into two terms of attraction and alignment which depend only on the relative state of both interacting agents: $\delta\phi_{ij}(d_{ij}, \psi_{ij}, \phi_{ij}) = \delta\phi_\mathrm{Att}(d_{ij}, \psi_{ij}, \phi_{ij}) + \delta\phi_\mathrm{Ali}(d_{ij}, \psi_{ij}, \phi_{ij})$, where d_{ij} is the distance between fish i and fish j, ψ_{ij} is the angle with which fish i perceives fish j, and $\phi_{ij} = \phi_j - \phi_i$ is the difference of heading or alignment.

We thus define the **influence** of a neighbor j on a focal individual i as the absolute contribution of the neighbor to the instantaneous heading change of the focal individual $\delta\phi_i(t)$ in Eq. (4), that is, for $j = 1, \ldots, N$, $j \neq i$:

$$\mathcal{I}_{ij}(t) = \left|\delta\phi^{ij}_{\mathrm{Att}}(t) + \delta\phi^{ij}_{\mathrm{Ali}}(t)\right|. \tag{7}$$

We assume that both the attraction and the alignment functions can be decoupled. Thus, we have $\delta\phi_{\mathrm{Att}}(d_{ij}, \psi_{ij}, \phi_{ij}) = F_{\mathrm{Att}}(d_{ij})\, O_{\mathrm{Att}}(\psi_{ij})\, E_{\mathrm{Att}}(\phi_{ij})$, where

$$F_{\mathrm{Att}}(d) = \gamma_{\mathrm{Att}} \left(\frac{d}{d_{\mathrm{Att}}} - 1\right) \frac{1}{1 + (d/l_{\mathrm{Att}})^2}, \tag{8}$$

$$O_{\mathrm{Att}}(\psi) = \beta_{\mathrm{Att}} \sin(\psi)\Big(1 - 0.33\cos(\psi)\Big), \tag{9}$$

$$E_{\mathrm{Att}}(\phi) = \lambda_{\mathrm{Att}}\Big(1 - 0.48\cos(\phi) - 0.31\cos(2\phi)\Big). \tag{10}$$

Here $d_{\mathrm{Att}} = 3$ cm is the distance at which the short-range repulsion of individual collision avoidance balances the long-range repulsion, $\gamma_{\mathrm{Att}} = 0.12$ is the intensity of the interaction, and $l_{\mathrm{Att}} = 20$ cm its range of action. The angular functions O_{Att} and E_{Att} are respectively normalized with $\beta_{\mathrm{Att}} = 1.395$ and $\lambda_{\mathrm{Att}} = 0.9326$.

In the alignment, we have $\delta\phi_{\mathrm{Ali}}(d_{ij}, \psi_{ij}, \phi_{ij}) = F_{\mathrm{Ali}}(d_{ij})\, E_{\mathrm{Ali}}(\psi_{ij})\, O_{\mathrm{Ali}}(\phi_{ij})$, where

$$F_{\mathrm{Ali}}(d) = \gamma_{\mathrm{Ali}} \left(\frac{d}{d_{\mathrm{Ali}}} + 1\right) \exp\left[-\left(\frac{d}{l_{\mathrm{Ali}}}\right)^2\right], \tag{11}$$

$$E_{\mathrm{Ali}}(\psi) = \beta_{\mathrm{Ali}}\Big(1 + 0.6\cos(\psi) - 0.32\cos(2\psi)\Big), \tag{12}$$

$$O_{\mathrm{Ali}}(\phi) = \lambda_{\mathrm{Ali}} \sin(\phi)\Big(1 + 0.3\cos(2\phi)\Big), \tag{13}$$

with $d_{\mathrm{Ali}} = 6$ cm, $l_{\mathrm{Ali}} = 20$ cm, $\gamma_{\mathrm{Ali}} = 0.09$, $\beta_{\mathrm{Ali}} = 0.9012$, $\lambda_{\mathrm{Ali}} = 1.6385$.

The parameter values given in the text are those derived in [14] for the simulation model when fish swim in pairs. More details of the model, including the derivation of the above functions, can be found in [14].

Computational model in an unbounded space

Model simulations of agents swimming in an unbounded space were carried out by removing the interaction with the wall (*i.e.*, by setting $\gamma_{\mathrm{w}} = 0$; the rest of parameter values being those given in Table 1.

For each strategy of interaction, that is, paying attention to the k most influential neighbors or to the k-nearest neighbors, for $k = 1$, 2, 3 and 4, and the case where agents do not interact with each other ($k = 0$), group cohesion is averaged over a large number of simulation runs n: $\langle C(t)\rangle = (1/n)\sum_{i=1}^{n} C_i(t)$, where $C_i(t)$ is the group cohesion at time t in the i-th run. We used $n = 1000$. The duration of each simulation was sufficiently long to produce a total number of 10^4 kicks per run among the 5 agents (~ 2.7 hours). A second series of simulations was carried out to produce 5×10^4 kicks (~ 13.5 hours), finding the same qualitative results. Initial conditions of each run were always different, with all agents located at less than $R = 25$ cm (the radius of the arena) from the origin of coordinates.

Three methods were considered to analyze the effect of reducing the attraction range: *i*) truncating the attraction intensity function F_{Att} to zero when the neighboring agent is further than a distance d_{cut} from the focal agent, $F_{\mathrm{Att}} = 0$ if $d_{ij} > d_{\mathrm{cut}}$; *ii*) varying the interaction range l_{Att}, and *iii*) varying the distance at which $F_{\mathrm{Att}}(d)$ reaches its maximum but preserving the value of the maximum. We found that the three methods gave rise to the same qualitative result and report here only the results of the first one.

For each value of d_{cut}, we calculated the mean cohesion as the average over the last 10% of kicks over the 1000 runs carried out to obtain $\langle C(t)\rangle$, and this, for each strategy and each value of k. When d_{cut} is sufficiently large, the attraction range is sufficiently long and $\langle C(t)\rangle$ is close to the value corresponding to the mean cohesion of the group when F_{Att} is not truncated. When d_{cut} is excessively small, the attraction range is so short that the agents simply diffuse and $\langle C(t)\rangle$ grows until the value corresponding to the case where there is no interaction between agents is reached. Both ranges of d_{cut} are separated by a critical value d^*_{cut}, whose precise value depends on the duration of the realizations, *i.e.*, on the number of kicks, that we fixed to 10^4 for Fig. 10.

Implementation of the behavioral model in the robots

We designed an Object-Oriented Programming software tool (OOP) for the distributed control of the Cuboids robots (Fig. 13). It first establishes independent memories for each robot as an agent to store their real time information, such as robot ID, location $\vec{u}^{\,n}(x^n, y^n)$ and heading ϕ^n at time step n, and position of the target place $\vec{u}^{\,n+1}$ at time step $n+1$. The OOP software provides a state machine control structure to generate for each individual robot the position of their target place and then it dispatches the control signals to the robots. With the new target place determined by the proposed strategy, the actuators of the robot are controlled wirelessly by WIFI signals sent by the computer. The robot controls its wheels to move towards the new target place while LED colors display the state of the robot.

Robots use a constant kick length of around 8 cm, that is, twice the body length of a robot, which corresponds to the mean kick length measured in experiments with five fish. Using a constant straight step also allows to check if the new target place can be reached or not, in particular, to prevent the case where the agent could be intercepted by another agent, in which case the distance traveled by the agent will be shorter than l_i^n.

The distributed control structure was designed to test the different local interaction strategies among the robot. The decision structure for an individual robot includes two main states: COMPUTE state and MOVE state (Fig. 14).

The robots are programmed to perform a burst-and-coast movement mimicking the swimming mode of the fish. When a robot is in the COMPUTE state it computes a new target place based on the current local interaction strategy. After that, the robot switches to the MOVE state, where the robot adjusts its wheels to move towards the target place. Since other robots are moving around asynchronously, the robot must avoid these dynamic obstacles while being in the MOVE state. To prevent collisions between robots, we designed and implemented an obstacle avoidance protocol. When no valid targets can be generated during the COMPUTE state (due to the impediment imposed by nearby robots), the robot generates a valid target place by means of a scanning method and, alternatively, just moves back a short distance.

We describe below the two states and the additional procedures used to avoid collisions with dynamical obstacles.

- COMPUTE State: This state generates a new target place for the focal robot by means of the proposed strategies, which are programmed in MATLAB. In this state, the robot takes the information about its local environment and selects the neighbors to be taken into account corresponding to the current local interaction strategy. Then the robot computes the variation of its heading angle according to the computational model and determines a new place target. The new target place is then checked and validated by the OOP software so as to avoid any collision with static obstacles, before the robot switches to the MOVE state (see Fig. 14). While a robot is in the COMPUTE State, the white LED light is turned on.

- MOVE State: In this state the robot evaluates whether its heading angle is aligned with the new pace target. If the deviation is too large, the robot first rotates towards the target and then moves straight until it reaches the target. Then, when the robot successfully reaches the target, it returns to the COMPUTE state to determine a new target place. While a robot is in the MOVE State, the green LED light is turned on.

- Obstacle Avoidance Protocol: This procedure is triggered as soon as the target path of the focal robot crosses the safety zone of another robot. The safety zone is a circular area around a robot with diameter of 80 mm. In this case, the focal robot first stops and computes whether it can continue moving or not according to the information it has about the distance d and relative angular position ψ of the neighboring robot. If the focal robot has the moving priority (determined by a large value of the angle of perception, $\psi > 90°$, meaning that the robot is "behind"), or if the distance is larger than the diameter of the circle of security ($d > 80$ mm, meaning that the robot sufficiently far), the moving condition is satisfied and the focal robot successfully turns back into the MOVE state. If not, the focal robot repeatedly checks the values d and ψ of the neighboring robot until the moving condition is satisfied. If the focal robot cannot go back into the MOVE state within 3 seconds, it toggles to the COMPUTE state to determine a new target place.

- No Valid Target Procedure: This procedure is triggered when the robot is in the COMPUTE state and cannot generate a valid target place within 3 seconds. In this situation, the robot scans the local environment from its front to the nearest neighbor located at one of its sides. If there exists a free space for generating a target place, the robot toggles to the MOVE state. If, after scanning, no free space is available for moving, the robot moves back over a predefined distance of 80 mm (approximately two robot body lengths) and then turns into the COMPUTE state to determine a new target place.

Local interactions strategies

In order to coordinate their motion with those of its neighbors, agents and robots have to select the relevant neighbors with which they interact, then compute the effect of social interactions, and finally sum up these effects to get the resultant heading angle variation.

In a group of 5 agents, there exist many ways for an agent to select the influential neighbors. We investigated the impact of three different strategies for an agent to interact with k of its $N - 1 = 4$ neighbors. A first strategy consists in selecting the neighbors according to their distance to the focal agent. A second strategy, included in our study as a control or a null strategy, consists in choosing randomly k neighbors to interact with. The third strategy consists in interacting with the agents that have the largest influence on the focal agent, where the influence is defined by the absolute contribution of the neighbor to the total heading variation of the focal agent, that is, the largest value of $|\delta\phi_{ij}|$; see equation (7).

For each kind of strategy, we consider that the focal individual can interact with $k = 1$, 2 or 3 neighbors. We also considered the case where agents interact with all the other individuals ($k = 4$), and finally, we tested the condition in which there is no social interaction between agents (*i.e.*, no attraction nor alignment, only collision avoidance in robots), a situation that corresponds to a null model ($k = 0$) with respect to social interactions. For each combination of interactions, we performed 50 simulations for a total of 8×10^4 kicks for all the 5 agents (about 21 hours per condition) and 1 robotic experiment with about 8000 kicks in average for all the 5 robots (about 1 hour per condition).

Quantification of collective behavior

We characterize the collective behavioral patterns by means of six quantities relative to the behavior of the group in the tank and to the behavior of individuals inside the group. To do that, we first write the coordinates of the position $\vec{u}_B = (x_B, y_B)$ and the velocity $\vec{v}_B = (v_B^x, v_B^y)$ of the point B corresponding to the center of mass or barycenter of the group with respect to the reference system of the tank. That is,

$$x_B(t) = \frac{1}{N}\sum_{i=1}^{N} x_i(t), \quad v_B^x(t) = \frac{1}{N}\sum_{i=1}^{N} v_i^x(t). \tag{14}$$

We omit the expressions of y_B and v_B^y because they are identical. The heading of the barycenter is then given by $\phi_B = \mathtt{ATAN2}(v_B^y, v_B^x)$.

The barycenter defines a system of reference in which the relative position and velocity of a fish, that we denote with a bar, are such that $\bar{x}_i = x_i - x_B$ and $\bar{v}_{x,i} = v_{x,i} - v_{x,B}$ (same expressions for the y-components). In the reference system of the barycenter, the angle of the position of a fish is given by $\bar{\theta}_i = \mathtt{ATAN2}(\bar{y}_i, \bar{x}_i)$, so the relative heading in this reference system is $\bar{\phi}_i = \mathtt{ATAN2}(\bar{v}_{y,i}, \bar{v}_{x,i}) \neq \phi_i - \phi_B$. We can thus define the angle of incidence of a fish with respect to a circle centered in the barycenter as $\bar{\theta}_{\mathrm{w},i} = \bar{\phi}_i - \bar{\theta}_i$. The angle $\bar{\theta}_{\mathrm{w},i}$ is the equivalent to the angle of incidence to the wall $\theta_{\mathrm{w},i}$ that we use in the reference system of the tank, and serves to measure the angular velocity of a fish with respect to the barycenter, in the reference system of the barycenter.

The six quantities are thus defined as follows:

1. Group cohesion $C(t) \in [0, R]$:

$$C(t) = \sqrt{\frac{1}{N}\sum_{i=1}^{N} \|\vec{u}_i - \vec{u}_B\|^2}, \tag{15}$$

   where $\|\vec{u}_i - \vec{u}_B\|$ is the distance from fish i to the barycenter B of the N fish.

   Low values of $C(t)$ correspond to highly cohesive groups, while high values of $C(t)$ denote that individuals are spatially dispersed.

2. Group polarization $P(t) \in [0, 1]$:

$$P(t) = \frac{1}{N}\left\|\sum_{i=1}^{N} \vec{e}_i(t)\right\|, \tag{16}$$

   where $\vec{e}_i = \vec{v}_i/\|\vec{v}_i\| = (\cos(\phi_i), \sin(\phi_i))$ is the unit vector in the direction of motion of the individual fish, given by its velocity vector $\vec{v}_i$.

   The polarization is thus the norm of the resultant of N vectors. A value of P close to 1 would mean that the N vectors are aligned and point in the same direction, while a value of P close to 0 would mean that the N vectors point in different directions, but can also mean that vectors are collinear and with opposite direction (*e.g.*, for N even, half of the vectors point North, the other half point South) so that they cancel each other. Similarly, when $N = 5$ and two normalized velocity vectors cancel each other (*e.g.*, when 4 fish swim in the same direction $\vec{e}$ and one fish swims in the opposite direction $-\vec{e}$) would give rise to a resultant vector of norm $P = (4 \times 1 - 1)/5 = 3/5 = 0.6$, and if two pairs of fish cancel each other, then $P = (3 \times 1 - 2 \times (-1))/5 = 1/5 = 0.2$.

3. Mean distance to the wall $\langle r_{\mathrm{w}} \rangle (t) \in [0, R]$:

$$\langle r_{\mathrm{w}} \rangle (t) = \frac{1}{N} \sum_{i=1}^{N} r_{\mathrm{w},i}(t), \tag{17}$$

Note that when the individuals move in a cohesive group, $\langle r_{\mathrm{w}} \rangle$ is typically of the same order as the distance of the barycenter to the wall $r_{\mathrm{w},B}$.

4. Relative angle of the barycenter heading to the wall $\theta_{\mathrm{w},B}(t) \in [-\pi, \pi]$:

$$\theta_{\mathrm{w},B}(t) = \mathtt{ATAN2}(v_{y,B}(t), v_{x,B}(t)). \tag{18}$$

5. Index of rotation $\Gamma(t) \in [-1, 1]$ around the center of the tank T:

$$\Gamma(t) = \frac{1}{N} \sum_{i=1}^{N} \sin(\theta_{\mathrm{w},i}(t)). \tag{19}$$

The index of rotation of a single fish with respect to the center of the tank is given by the relative angle with the wall $\theta_{\mathrm{w},i}$. In fact, $\theta_{\mathrm{w},i} > 0$ means that the fish is swimming counter-clockwise (CCW) with respect to the center of the tank, and $\theta_{\mathrm{w},i} < 0$ means that the fish is swimming clockwise (CW). Thus, $\Gamma(t)$ is actually the mean index of rotation of the group: if $\Gamma(t) > 0$ then the group is rotating CCW, and if $\Gamma(t) < 0$ then rotation is CW.

Fish swim most of the time parallel to the wall, so that $\Gamma(t)$ is the mean of N values that are most of the time close to $+1$ (but below) or -1 (but above). As happened for $P(t)$, fish can cancel each other: for instance, 4 fish swimming CWW and 1 CW would give $\Gamma = 0.6$, while 2 CWW and 3 CW would give $\Gamma = -0.2$. We have preserved the information given by the sign in order to track the number of changes of direction of the group.

6. Index of collective counter-milling and super-milling $Q(t) \in [-1, 1]$:

$$\begin{aligned} Q(t) &= \left(\frac{1}{N} \sum_{i=1}^{N} \sin(\bar{\theta}_{\mathrm{w},i}(t)) \right) \times \mathtt{SIGN} \left(\frac{1}{N} \sum_{i=1}^{N} \sin(\theta_{\mathrm{w},i}(t)) \right) \quad (20) \\ &= \Gamma_B(t) \times \mathtt{SIGN}\big(\Gamma(t)\big). \quad (21) \end{aligned}$$

A group of fish rotating around the center of the tank with a rotation index $\Gamma(t)$ would display a counter-milling behavior if the individual fish also rotate around the barycenter of the group they form and both directions of rotation are opposite. The first sum between parentheses in (20) is the index of rotation of fish with respect to the barycenter of the group, denoted by $\Gamma_B(t)$ in (21). Multiplying by the sign of $\Gamma(t)$ means that when $Q(t) < 0$ then both directions are opposite and fish exhibit a *collective counter-milling behavior*, while when $Q(t) > 0$, both rotations are in the same direction and fish exhibit a *collective super-milling behavior*.

Thus, a group of 5 individuals turning around the center of the tank in a rigid formation that always points North, like the fingertips of the hand when cleaning a window, would correspond to a counter-milling behavior. In turn, a situation where individuals rotate around the center of the tank as if they were fixed to a vinyl record, so that trajectories are perfect circles and individuals far from the center of the tank move faster than those close to the center, would correspond to a zero-milling state; what fish do is something in-between (see Fig. 3 for fish, and S4 Video for robots).

Collective behavior is thus quantified by means of the probability density functions of these quantities. In addition, density maps are used to illustrate the variation of polarization and rotation index with respect to cohesion. We consider two normalizations: *i*) with the total number of data, to highlight the significant regions of the map and neglect the regions where the data are scarce, and *ii*) with the total number of data in a range of the polarization or the rotation index (*i.e.*, each row in the map is a PDF). Spatial distances are scaled with the corresponding values of $\lambda_{\mathrm{M}} = 0.87$ and $\lambda_{\mathrm{R}} = 0.35$, and we also calculated two versions of the rotation index, with and without adding specular trajectories.

Acknowledgments

L.L. was supported by a grant from the Natural Science Foundation of Shanghai under grant No. 17ZR1419000. This study was supported by grants from the Centre National de la Recherche Scientifique (CNRS) and University Paul Sabatier (project Dynabanc).

References

1. D.J.T. Sumpter (2010). Collective Animal Behavior. Princeton, NJ: Princeton University Press.

2. I.D. Couzin (2002). Collective cognition in animal groups. Trends in Cognitive Science, 13(1):36433.

3. M. Moussaïd, S. Garnier, G. Theraulaz and D. Helbing (2009). Collective information processing in swarms, flocks and crowds. Topics in Cognitive Science 1, 469–497.

4. S. Camazine, J.L. Deneubourg, N. Franks, J. Sneyd, G. Theraulaz and E. Bonabeau (2001). Self-Organization in Biological Systems. Princeton, NJ: Princeton University Press.

5. I.D. Couzin and J. Krause (2003). Self-organization and collective behavior in vertebrates. Advances in the Study of Behavior 32: 1–75.

6. U. Lopez, J. Gautrais, I.D. Couzin and G. Theraulaz (2012). From behavioural analyses to models of collective motion in fish schools. Interface Focus 2:693-707.

7. A. Cavagna, A. Cimarelli, I. Giardina, G. Parisi, R. Santagati, F. Stefanini and R. Tavarone (2010). From empirical data to inter-individual interactions: unveiling the rules of collective animal behavior. Mathematical Models and Methods in Applied Sciences 20:1491–1510.

8. D.J.T. Sumpter (2006). The principles of collective animal behaviour. Philosophical Transactions of the Royal Society B: Biological Sciences 361 (1465):5–22.

9. T. Sasaki and S.C. Pratt (2018). The Psychology of Superorganisms: Collective Decision Making by Insect Societies. Annual Review of Entomology 63:259–275.

10. C. Detrain and J.L. Deneubourg (2006). Self-organized structures in a superorganism: Do ants "behave" like molecules? Physics of Life Reviews 3(3):162–187.

11. C. Detrain and J.L. Deneubourg (2008). Collective decision-making and foraging patterns in ants and honeybees. Advances in Insect Physiology 35:123–173.

12. T.D. Seeley (1996). Wisdom of the Hive. Cambridge, MA: Harvard Univ. Press.

13. T.D. Seeley (2010). Honeybee Democracy. Princeton, NJ: Princeton Univ. Press.

14. D.S. Calovi, A. Litchinko, V. Lecheval, U. Lopez, A. Pérez Escudero, H. Chaté, C. Sire, G. Theraulaz (2018). Disentangling and modeling interactions in fish with burst-and-coast swimming reveal distinct alignment and attraction behaviors. PLoS Comput. Biol. 14(1):e1005933.

15. J.K. Parrish, S.V. Viscido and D. Grunbaum (2002). Self-organized fish schools: An examination of emergent properties. Biological Bulletin 202:296–305.

16. T. Vicsek and A. Zafeiris (2012). Collective motion. Physics Reports 517: 71–14.

17. I. Aoki (1982). A simulation study on the schooling mechanism in fish. Bull. J. Soc. Sci. Fish 48(8):1081–1088.

18. I. D. Couzin, J. Krause, R. James, G. Ruxton and N. Franks (2002) Collective memory and spatial sorting in animal groups. J. Theor. Biol. 218(5):1–11.

19. T. Vicsek, A. Czirók, E. Ben-Jacob, I. Cohen and O. Shochet (1995). Novel Type of Phase Transition in a System of Self-Driven Particles. Physical Review Letters 75: 226–1229.

20. M. Ballerini et al.(2008). Interaction Ruling Animal Collective Behavior Depends on Topological Rather than Metric Distance: Evidence from a Field Study. Proc. Natl. Acad. Sci. USA 105:1232-1237.

21. M. Camperi, A. Cavagna, I. Giardina, G. Parisi and E. Silvestri (2012). Spatially balanced topological interaction grants optimal cohesion in flocking models. Interface Focus 2:715–725.

22. J. Gautrais *et al.* (2012). Deciphering interactions in moving animal groups. PLoS Comp. Biol. 8(9):e1002678.

23. A. Strandburg-Peshkin, D.R. Farine, I.D. Couzin and M.C. Crofoot (2015). Shared decision-making drives collective movement in wild baboons. Science 348:1358–1361.

24. B.H. Lemasson, J.J. Anderson and R.A. Goodwin (2009). Collective motion in animal groups from a neurobiological perspective: the adaptive benefits of dynamic sensory loads and selective attention. Journal of Theoretical Biology 261(4):501–510.

25. B.H. Lemasson, J.J. Anderson and R.A. Goodwin (2013). Motion-guided attention promotes adaptive communication during social navigation. Proceedings of the Royal Society of London B: Biological Sciences 280(1754):20122003.

26. A.M. Calvao and E. Brigatti (2014). The Role of Neighbours Selection on Cohesion and Order of Swarms. PLoS ONE 9(5): e94221.

27. L. Jiang, L. Giuggioli, A. Perna, R. Escobedo, V. Lecheval, C. Sire, Z. Han and G. Theraulaz (2017). Identifying influential neighbors in animal flocking. PLoS Comput. Biol. 13:e1005822.

28. Y. Katz, K. Tunstrøm, C. Ioannou, C. Huepe and I. D. Couzin (2011). Inferring the structure and dynamics of interactions in schooling fish. Proc. Natl. Acad. Sci. USA 108(46):18720–18725.

29. A.E. Turgut, H. Çelikkanat, F. Gökçe and E. Şahin (2008). Self-organized flocking in mobile robot swarms. Swarm Intelligence 2:97–120.

30. C. Muro, R. Escobedo, L. Spector and R.P. Coppinger (2011). Wolf-pack (*Canis lupus*) hunting strategies emerge from simple rules in computational simulations. Behav. Processes 88(3):192–197.

31. R. Dukas (2002). Behavioural and ecological consequences of limited attention. Phil. Trans. R. Soc. Lond. B 357:1539–1547.

32. C. Reynolds (1987). Flocks, herds and schools: A distributed behavioral model. Computer Graphics 21(4) (SIGGRAPH '87 Conference Proceedings), pp. 25–34.

33. A. Pérez-Escudero, J. Vicente-Page, R.C. Hinz, S. Arganda, and G.G. de Polavieja (2014). idTracker: tracking individuals in a group by automatic identification of unmarked animals. Nature Methods, 11:743–748.

34. J. Goncalves, J. Lima and P. Costa (2008). Real-time localization of an omnidirectional mobile robot resorting to odometry and global vision data fusion: An EKF approach.. IEEE International Symposium on Industrial Electronics, pp. 1275–1280.

35. X. Hu (2005). Applying robot-in-the-loop-simulation to mobile robot systems. In Advanced Robotics, 2005. ICAR'05 Proceedings, 12th International Conference on, pp. 506–513.

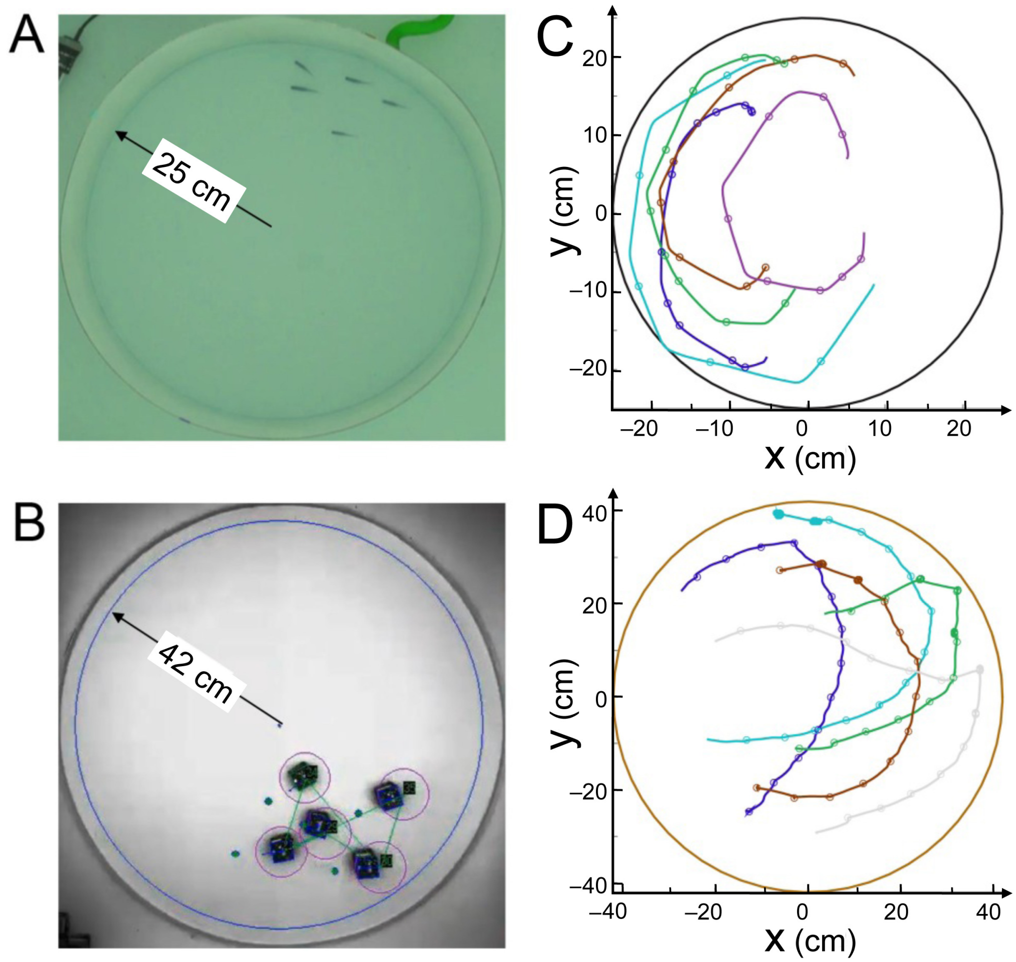

Fig 1. Experimental setups and tracking. (A) Experiments with 5 fish swimming in a tank of radius $R_{\mathrm{fish}} = 25$ cm. (B) 5 robots running in a platform of radius $R_{\mathrm{robot}} = 42$ cm. (C) Individual fish trajectories over 4 seconds. The circles represent the onset of bursts, when speed is minimum. (D) Individual trajectories in one robotic experiment over 24 seconds. The circles indicate the decisions of the robots to select a new target place, when individual speed is minimum.

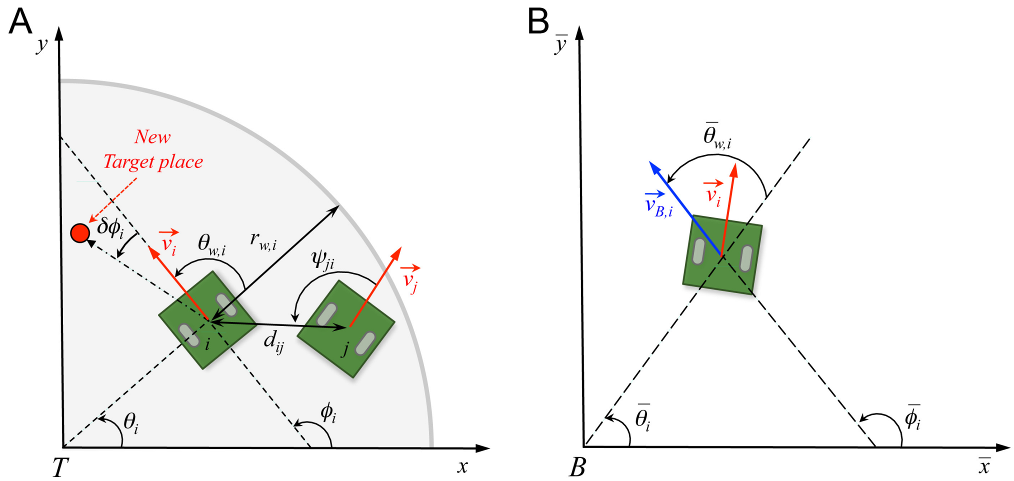

Fig 2. Angles and reference systems. (A) Distances, angles and velocity vectors of agents i and j in the absolute reference system centered in $T(0,0)$. Positive values of angles are fixed in the anticlockwise direction. Angle θ_i is the position angle of agent i with respect to T and the horizontal line; $r_{\mathrm{w},i}$ is the distance of agent i to the wall; ϕ_i is the heading of agent i, determined by its velocity vector $\vec{v}_i$; $\theta_{\mathrm{w},i}$ is the relative angle of agent i with the wall; d_{ij} is the distance between agents i and j; ψ_{ij} is the angle with which agent i perceives agent j; $\phi_{ij} = \phi_j - \phi_i$ is the difference of heading between agents i and j, and $\delta\phi_i$ is the variation of heading of agent i. (B) Relative reference system centered in the barycenter of the group $B(x_B, y_B)$. Relative variables are denoted with a bar. Angle $\bar{\theta}_{\mathrm{w},i} = \bar{\phi}_i - \bar{\theta}_i$ is the angle of incidence of the relative speed of agent i with respect to a circle centered in B.

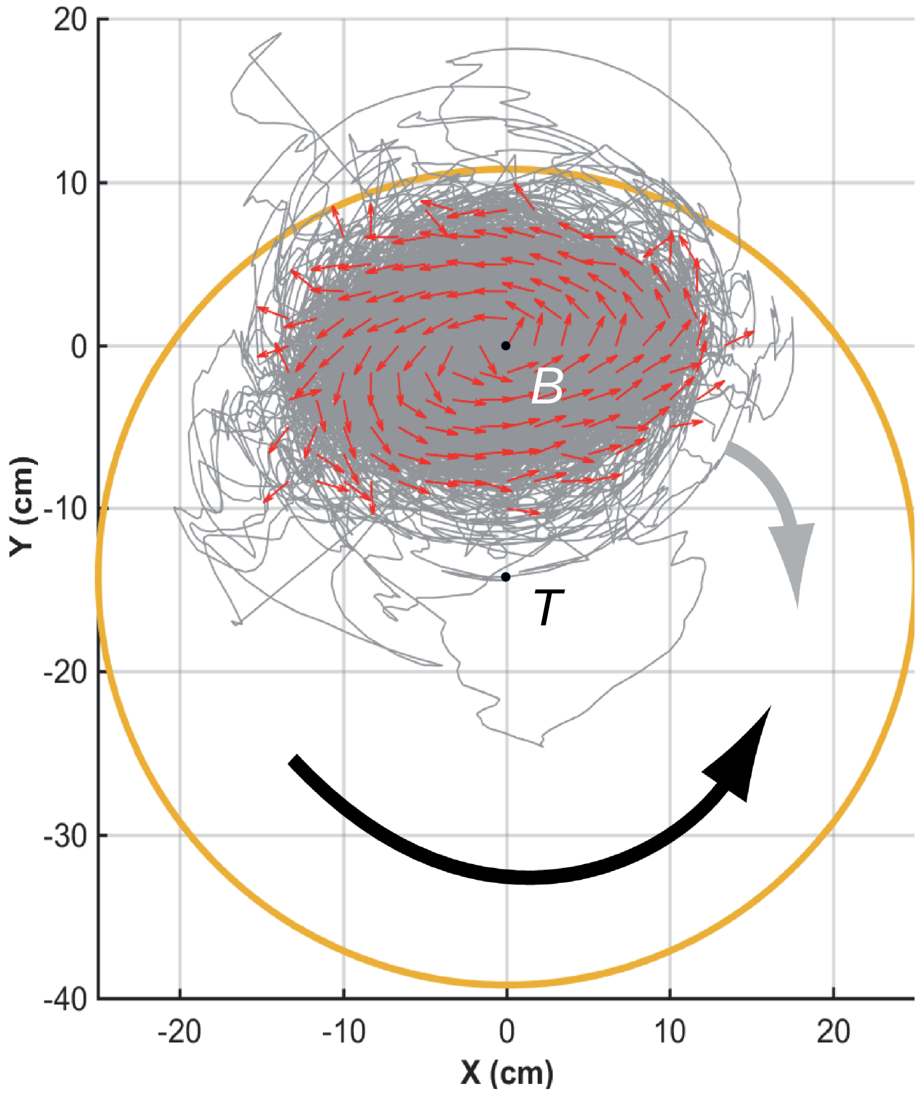

Fig 3. Counter-milling in fish experiments. Individual fish (small red arrows) turn counter-clockwise (CCW) around their barycenter, here located at $B(0,0)$, while fish group rotates clockwise (CW) around the center of the tank, located at $T(0,-14)$ in the reference system of the barycenter. Red arrows (of same length) denote relative fish heading, gray lines denote relative trajectories, and large orange circle denotes the average relative position of the border of the tank. The wide black arrow shows the direction of rotation of individual fish with respect to B (CCW), opposed to the wide gray arrow showing the direction of rotation of the group with respect to T (CW).

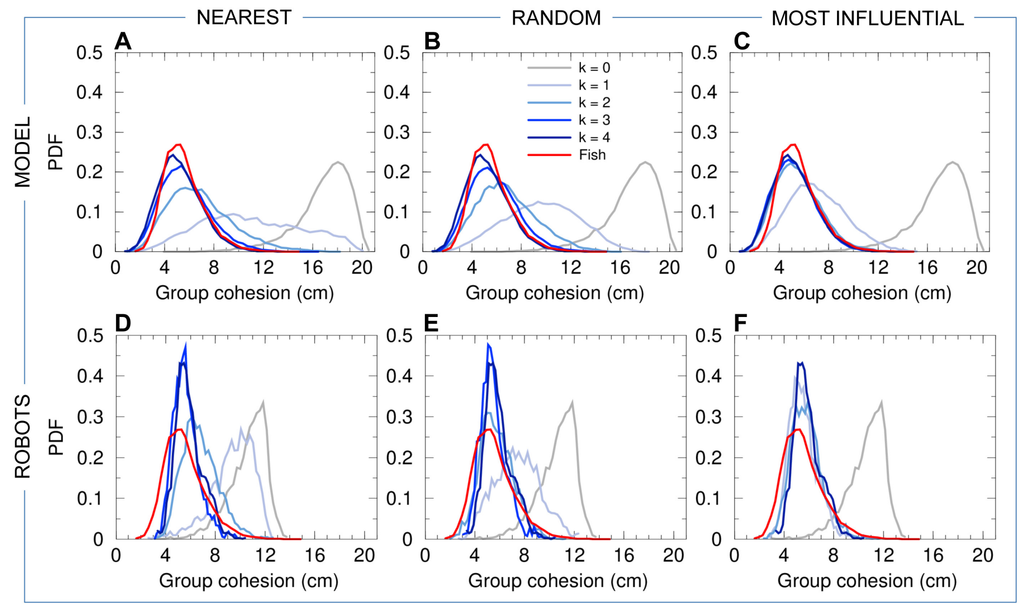

Fig 4. Group cohesion. Probability density functions (PDFs) of group cohesion $C(t)$ for the experiments with fish (red lines in all panels), model simulations (panels ABC) and experiments with swarm of robots (panels DEF), compared to the corresponding null models ($k = 0$, no interaction between individuals) in both simulations and robots (gray lines in all panels). Units are centimeters. Curves about agents (blue and gray lines) have been scaled with $\lambda_{\mathrm{M}} = 0.87$ for the model simulations and with $\lambda_{\mathrm{R}} = 0.35$ for robots. The PDFs (y-axis) are scaled accordingly to preserve the integral of the PDF equal to 1. The intensity of blue color is proportional to the number of neighbors with whom a individual (fish or robot) interacts, from $k = 1$ (light blue) to $k = 4$ (dark blue). The legend about lines' style shown in panel (B) is the same for the six panels. Strategies are, from left to right: panels A and D: nearest neighbors; B and E: random neighbors; C and F: most influential neighbors.

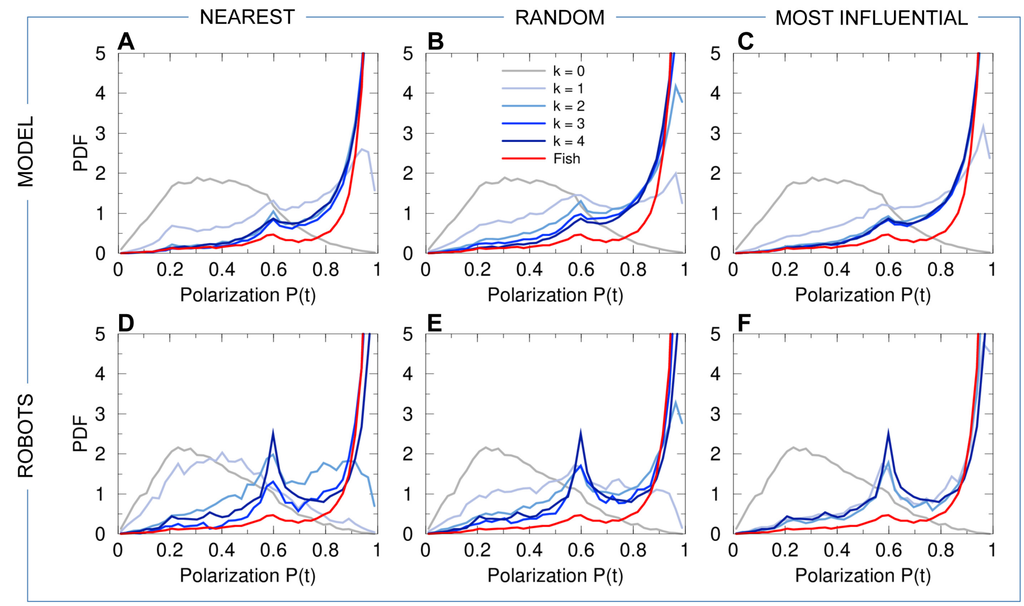

Fig 5. Group polarization. PDFs of group polarization $P(t)$ for the experiments with fish (red lines in all panels), model simulations (panels ABC) and experiments with robots (panels DEF), compared to the corresponding null models ($k = 0$, no interaction between individuals) in both simulations and robots (gray lines in all panels). Curves about agents (model and robots) are blue and gray lines. The intensity of blue color is proportional to the number of neighbors taken into account, from $k = 1$ (light blue) to $k = 4$ (dark blue). The legend about lines' style shown in panel (B) is the same for the six panels. Strategies are, from left to right: panels A and D: nearest neighbors; B and E: random neighbors; C and F: most influential neighbors.

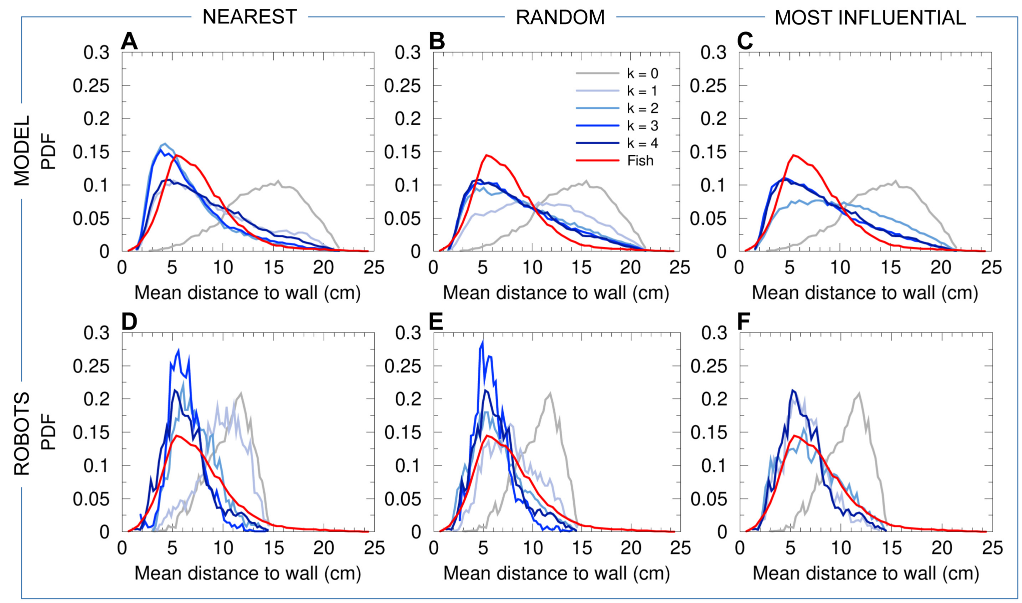

Fig 6. Mean distance of individuals to the border. PDFs of the mean distance of individuals to the wall $\langle r_\mathrm{w} \rangle$ for the experiments with fish (red lines in all panels), model simulations (panels ABC) and experiments with robots (panels DEF), compared to the corresponding null models ($k = 0$, no interaction between individuals) in both simulations and robots (gray lines in all panels). Units are centimeters. Curves about agents (blue and gray lines) have been scaled with $\lambda_\mathrm{M} = 0.87$ for the model simulations and with $\lambda_\mathrm{R} = 0.35$ for robots. The PDFs (y-axis) are scaled accordingly to preserve the integral of the PDF equal to 1. The intensity of blue color is proportional to the number of neighbors with whom an individual (fish or robot) interacts, from $k = 1$ (light blue) to $k = 4$ (dark blue). The legend about lines' style shown in panel (B) is the same for the six panels. Strategies are, from left to right: panels A and D: nearest neighbors; B and E: random neighbors; C and F: most influential neighbors.

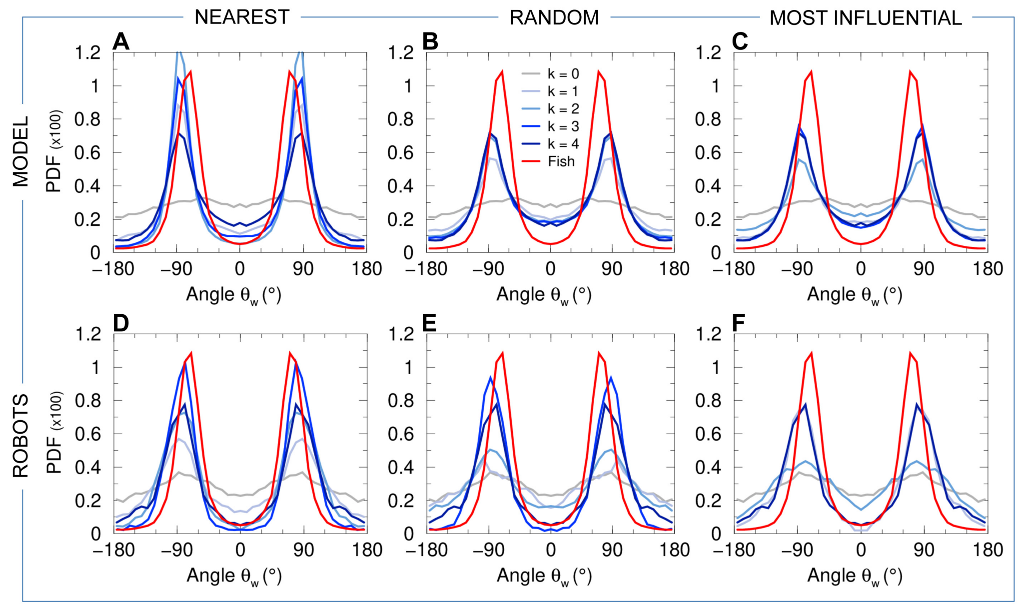

Fig 7. Relative angle of the heading of the barycenter of the group with the wall. PDFs of the relative angle of the heading of the barycenter of the group with the wall $\langle\theta_{\mathrm{w}}^{B}\rangle$ for the experiments with fish (red lines in all panels), model simulations (panels ABC) and experiments with robots (panels DEF), compared to the corresponding null models ($k = 0$, no interaction between individuals) in both simulations and robots (gray lines in all panels). Curves about agents (model and robots) are blue and gray lines. The intensity of blue color is proportional to the number of neighbors with whom an individual (fish or robot) interacts, from $k = 1$ (light blue) to $k = 4$ (dark blue). The legend about lines' style shown in panel (B) is the same for the six panels. Strategies are, from left to right: panels A and D: nearest neighbors; B and E: random neighbors; C and F: most influential neighbors.

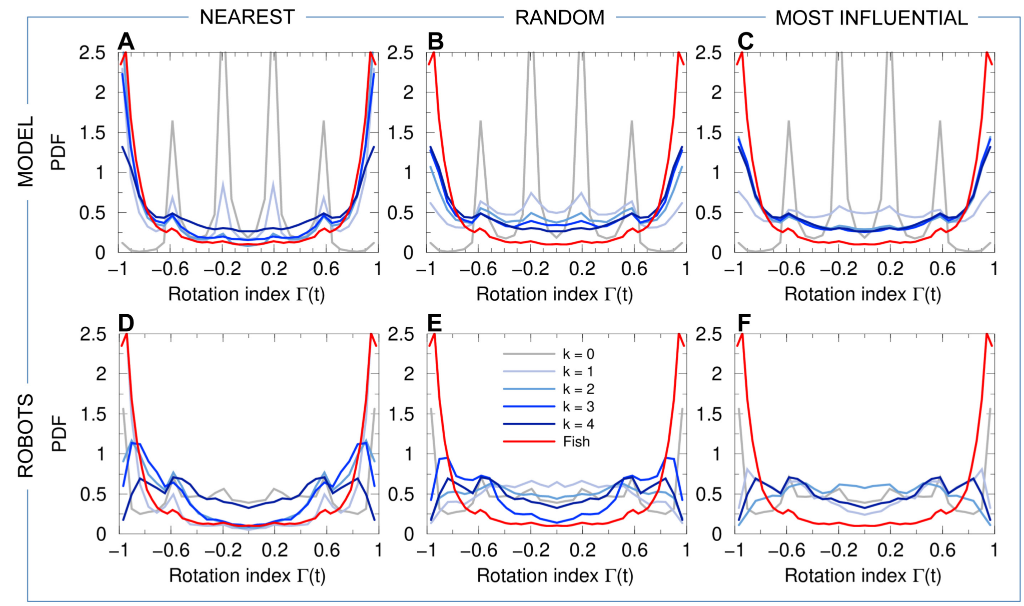

Fig 8. Index of rotation of the group around tank center. PDFs of rotation index $\Gamma(t)$ for the experiments with fish (red lines in all panels), model simulations (panels ABC) and experiments with robots (panels DEF), compared to the corresponding null models ($k = 0$, no interaction between individuals) in both simulations and robots (gray lines in all panels). Curves about agents (model and robots) are blue and gray lines. The intensity of blue color is proportional to the number of neighbors with whom an individual (fish or robot) interacts, from $k = 1$ (light blue) to $k = 4$ (dark blue). The legend about lines' style shown in panel (B) is the same for the six panels. Strategies are, from left to right: panels A and D: nearest neighbors; B and E: random neighbors; C and F: most influential neighbors.

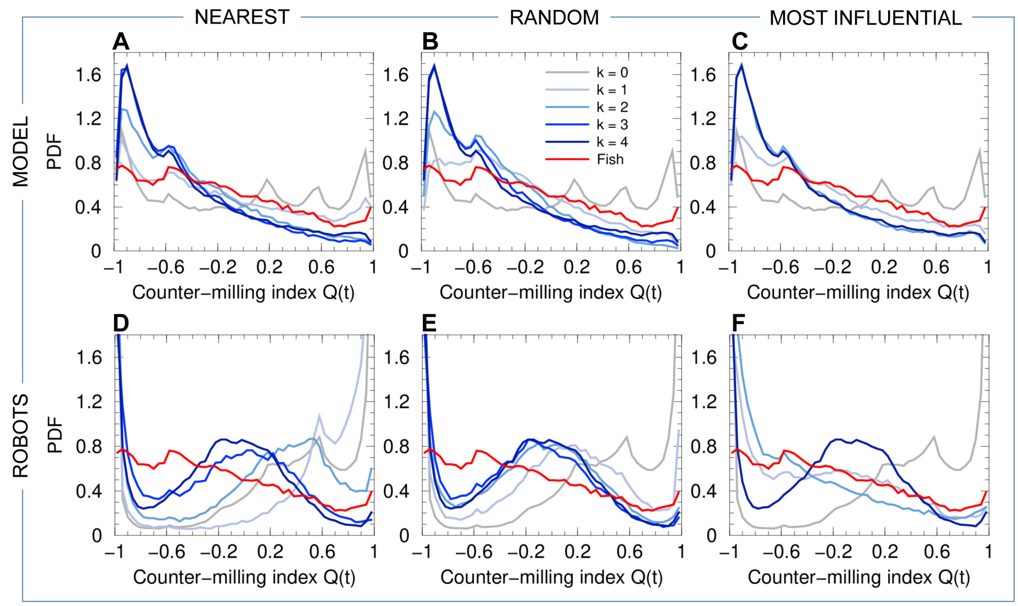

Fig 9. Counter-milling index. PDFs of the counter-milling index $Q(t)$ for the experiments with fish (red lines in all panels), model simulations (panels ABC) and experiments with robots (panels DEF), compared to the corresponding null models ($k = 0$, no interaction between individuals) in both simulations and robots (gray lines in all panels). Curves about agents (model and robots) are blue and gray lines. The intensity of blue color is proportional to the number of neighbors taken into account, from $k = 1$ (light blue) to $k = 4$ (dark blue). The legend about lines' style shown in panel (B) is the same for the six panels. Strategies are, from left to right: panels A and D: nearest neighbors; B and E: random neighbors; C and F: most influential neighbors.

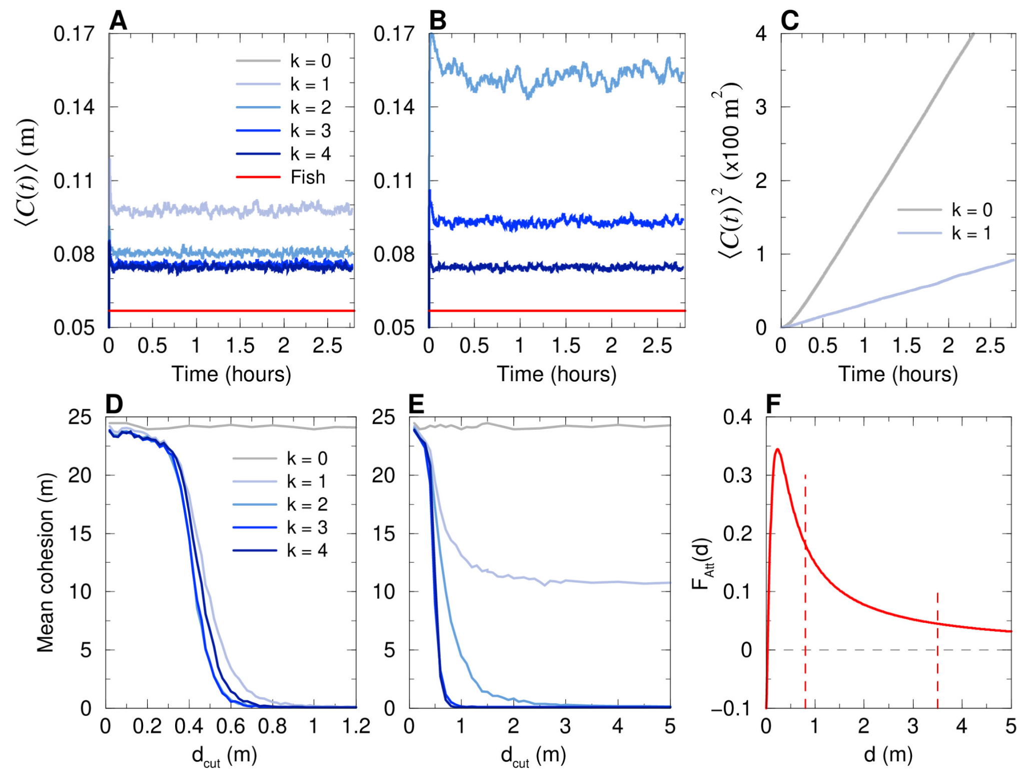

Fig 10. Average cohesion of a group of 5 agents swimming in an unbounded space. Model simulations of the two strategies, (AD) interacting with the k most influential neighbors, and (BCE) with the k nearest neighbors, for $k = 1, \ldots, 4$ (blue lines), together with the case with no interaction ($k = 0$, gray lines) and the mean cohesion of real fish in the tank (red lines in AB). (C): squared mean cohesion in the diffusive cases $k = 1$ nearest neighbor and $k = 0$, in an appropriate scale. (ABC): average of 1000 runs with 10000 kicks (≈ 2.7 hours) per run. (DE): Mean cohesion averaged over the last 10% of the 1000 runs for different values of the truncating distance d_{cut} for the two strategies: (D) Interacting with the most influential neighbors, and (E) with the nearest neighbors. Panel (F): Attraction function F_{Att} extended to long distances, showing the critical values of d_{cut} above which cohesion is preserved (vertical dashed lines): $d^*_{\mathrm{cut}} \approx 0.8$ m when the neighbors taken into account are the $k = 1$, 2 or 3 most influential ones, the $k = 3$ nearest ones or all the neighbors ($k = 4$), and $d^*_{\mathrm{cut}} \approx 3.5$ m when interacting with the two nearest ones (d^*_{cut} doesn't exist when interacting only with the nearest neighbor). When $d > 3.5$ m, the attraction is so weak that there is no gain in truncating F_{Att} beyond this value. Cohesion values are scaled with $\lambda_{\mathrm{M}} = 0.87$.

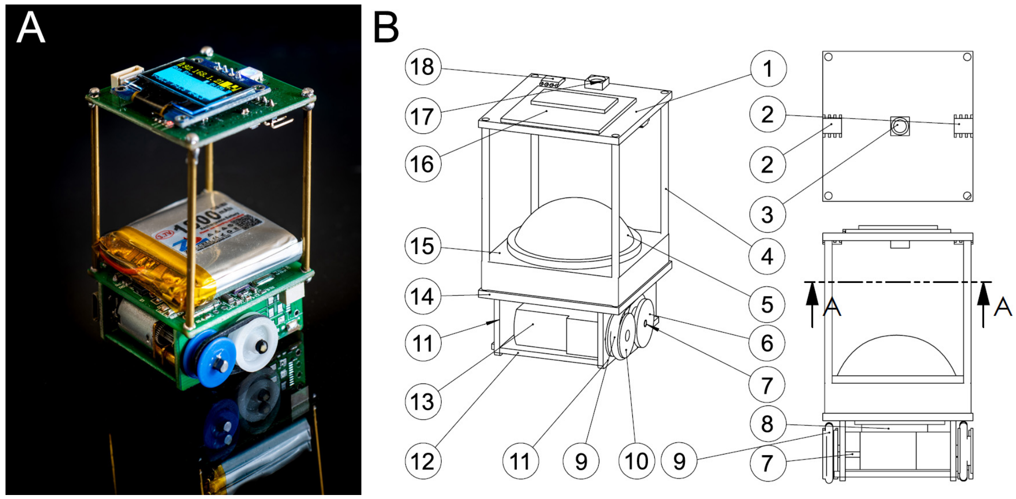

Fig 11. Cuboid robots. (A) Photograph of a Cuboid robot. Credits to David Villa ScienceImage/CBI/CNRS, Toulouse, 2018. (B) Design structure of Cuboid robot; A-A represents a cutaway view.

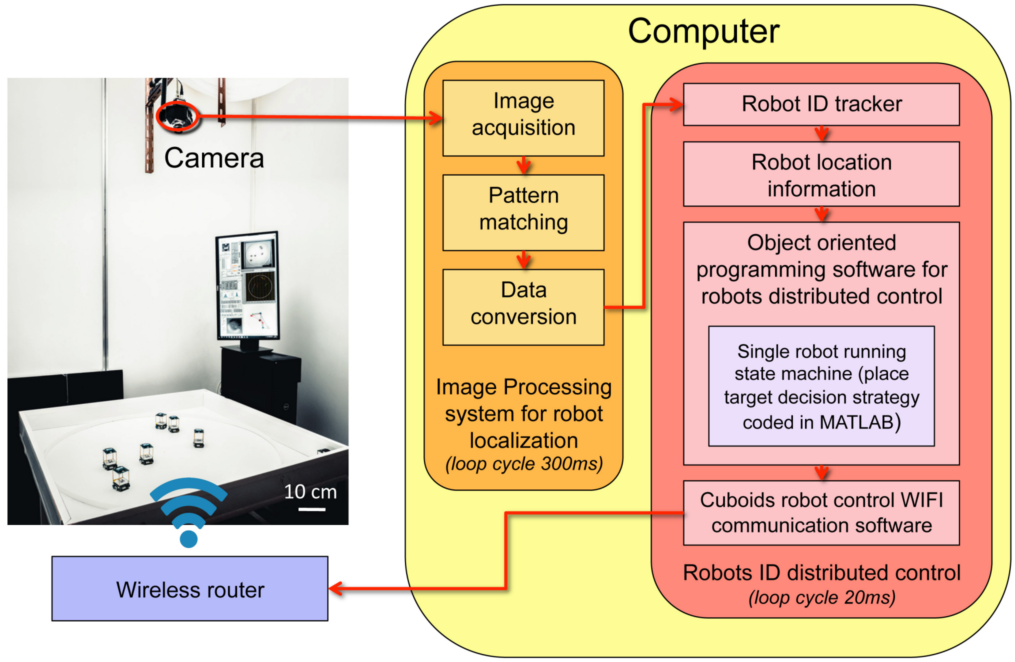

Fig 12. Structure of Cuboids swarm platform. Two main parts: the physical hardware and the control software. The hardware consists of a square platform. A camera mounted on the top of it to monitor the movements of Cuboids robots, which are controlled in a distributed way by a wireless router. The software processes the image acquired by the camera, then computed the actions to be performed by each robot, and finally sends the control signals to the robots via the wireless router. Credits to David Villa ScienceImage/CBI/CNRS, Toulouse, 2018.

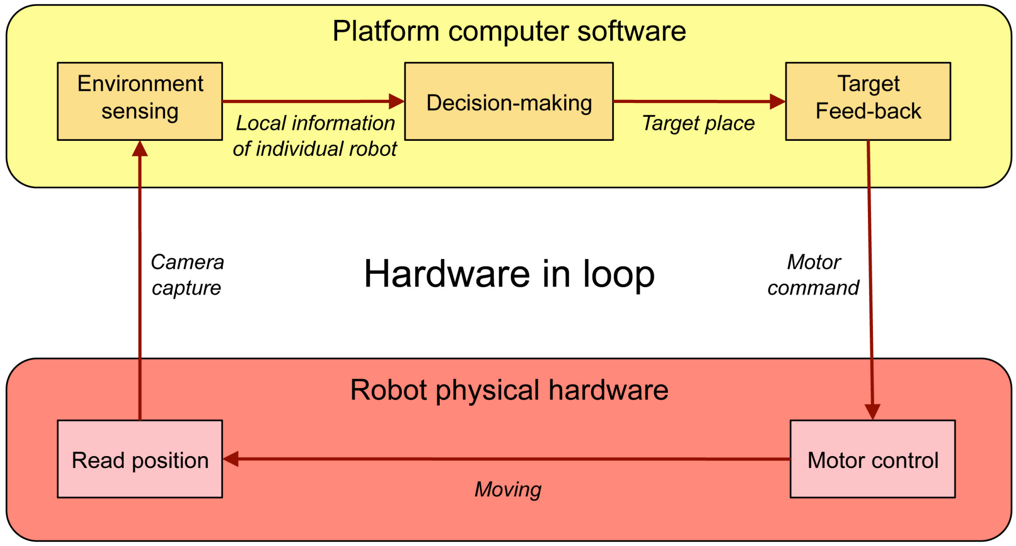

Fig 13. Hardware in Loop (HIL) simulation (from [35]). The structure of HIL consists of two parts: 1) Control Software and 2) Physical hardware. First the Control Software acquires the position of each robot. Then the Control Software generates a motor command for each robot based its local information. The robots receive theses motor commands and perform the corresponding movements that are monitored by the camera.

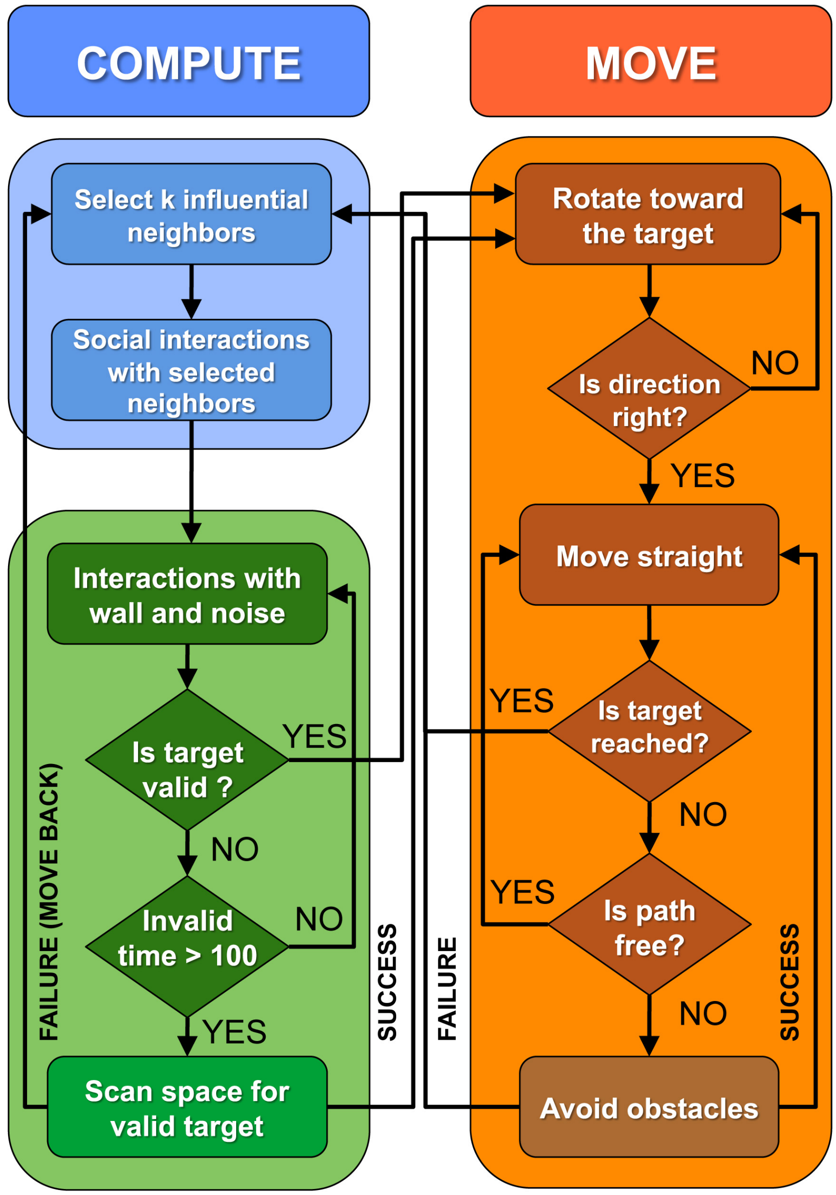

Fig 14. Flow chart of robot states machine. At any time a robot can be in one of the two following states: (1) the COMPUTE state for choosing a new target place, and (2) the MOVE state to reach the target place. In the COMPUTE state, the robot first selects influential neighbors, then it computes the pairwise influence of each neighbor, and finally it adds all influences to generate a new target place. Before moving, the choice of a valid target place is then validated to avoid collisions with the wall or another robot. If a valid target place cannot be found the robot scans all space for finding a valid target place. If the scanning method cannot find a valid target, the robot moves back over a distance of 80mm and starts again the COMPUTE state. When a valid target place has been found, the robot switches into the MOVE state. The robot first rotates towards to the target and then, moves straight to it. If another running neighbor blocks the path, the robot uses a procedure to avoid the obstacles.

Supporting Information

S1 Video. Collective movements in rummy-nose tetra (*Hemigrammus rhodostomus*). A typical experiment with a group of 5 fish swimming in a circular tank of radius 250 mm.

S2 Video. Collective motion in a group of 5 robots. Each robot interacts with its most influential neighbor. The video is accelerated 9 times. Total duration: 7.15 minutes.

S3 Video. Tracking and analysis output. The small circles superimposed on the trajectories represents the kicks performed by the fish when the speed reaches its maximum value.

S4 Video. Counter milling behavior in a group of 5 fish. Top: Typical experiment with a group of 5 fish in a circular arena of radius 250 mm. The video is accelerated 6 times. Total duration 1.3 minutes. Bottom: Relative movement of fish with respect to the barycenter of the group, represented by the black arrow on top video and a black disk on the bottom video. Fish turn counter-clockwise around the tank and clockwise with respect to the barycenter.

S5 Video. Swarm robotics experiment where there is no social interaction between the robots ($k = 0$) and only obstacle avoidance behavior is at play. Top: Typical experiment with a group of 5 robots in a circular arena of radius 420 mm, captured by the top camera. The border of the arena is represented by the red circle. Purple circles represent the individual robot safety area, of diameter 8 cm. Small green dots in front of robots indicate their next target place. The video is accelerated 6 times. Total duration: 6 minutes. Bottom: Relative movement of the robots with respect to the barycenter of the group. The barycenter is represented by the black disk and remains oriented to the right. Robots are represented by colored disks with their identification number in the center. The small circle at the front of a robot indicates its heading. The arrows represent the interactions between robots. Arrow direction indicates the identity (color) of the robot that exerts its influence on the robot to which the arrow points. The small dots in front of the robots represent the next target places.

S6 Video. Swarm robotics experiment where robots interact with the $k = 1$ nearest neighbor. Top: Typical experiment with a group of 5 robots in a circular arena of radius 420 mm, captured by the top camera. The border of the arena is represented by the red circle. Purple circles represent the individual robot safety area, of diameter 8 cm. Small green dots in front of robots indicate their next target place. The video is accelerated 6 times. Total duration: 6 minutes. Bottom: Relative movement of the robots with respect to the barycenter of the group. The barycenter is represented by the black disk and remains oriented to the right. Robots are represented by colored disks with their identification number in the center. The small circle at the front of a robot indicates its heading. The arrows represent the interactions between robots. Arrow direction indicates the identity (color) of the robot that exerts its influence on the robot to which the arrow points. The small dots in front of the robots represent the next target places.

S7 Video. Swarm robotics experiment where robots interact with the $k = 1$ most influential neighbor. Top: Typical experiment with a group of 5 robots in a circular arena of radius 420 mm, captured by the top camera. The border of the arena is represented by the red circle. Purple circles represent the individual robot safety area, of diameter 8 cm. Small green dots in front of robots indicate their next target place. The video is accelerated 6 times. Total duration: 6 minutes. Bottom: Relative movement of the robots with respect to the barycenter of the group. The barycenter is represented by the black disk and remains oriented to the right. Robots are represented by colored disks with their identification number in the center. The small circle at the front of a robot indicates its heading. The arrows represent the interactions between robots. Arrow direction indicates the identity (color) of the robot that exerts its influence on the robot to which the arrow points. The small dots in front of the robots represent the next target places.

S8 Video. Swarm robotics experiment where robots interact with $k = 1$ neighbor selected randomly. Top: Typical experiment with a group of 5 robots in a circular arena of radius 420 mm, captured by the top camera. The border of the arena is represented by the red circle. Purple circles represent the individual robot safety area, of diameter 8 cm. Small green dots in front of robots indicate their next target place. The video is accelerated 6 times. Total duration: 6 minutes. Bottom: Relative movement of the robots with respect to the barycenter of the group. The barycenter is represented by the black disk and remains oriented to the right. Robots are represented by colored disks with their identification number in the center. The small circle at the front of a robot indicates its heading. The arrows represent the interactions between robots. Arrow direction indicates the identity (color) of the robot that exerts its influence on the robot to which the arrow points. The small dots in front of the robots represent the next target places.

S9 Video. Swarm robotics experiment where robots interact with the $k = 2$ nearest neighbors. Top: Typical experiment with a group of 5 robots in a circular arena of radius 420 mm, captured by the top camera. The border of the arena is represented by the red circle. Purple circles represent the individual robot safety area, of diameter 8 cm. Small green dots in front of robots indicate their next target place. The video is accelerated 6 times. Total duration: 6 minutes. Bottom: Relative movement of the robots with respect to the barycenter of the group. The barycenter is represented by the black disk and remains oriented to the right. Robots are represented by colored disks with their identification number in the center. The small circle at the front of a robot indicates its heading. The arrows represent the interactions between robots. Arrow direction indicates the identity (color) of the robot that exerts its influence on the robot to which the arrow points. The small dots in front of the robots represent the next target places.

S10 Video. Swarm robotics experiment where robots interact with the $k = 2$ most influential neighbor. Top: Typical experiment with a group of 5 robots in a circular arena of radius 420 mm, captured by the top camera. The border of the arena is represented by the red circle. Purple circles represent the individual robot safety area, of diameter 8 cm. Small green dots in front of robots indicate their next target place. The video is accelerated 6 times. Total duration: 6 minutes. Bottom: Relative movement of the robots with respect to the barycenter of the group. The barycenter is represented by the black disk and remains oriented to the right. Robots are represented by colored disks with their identification number in the center. The small circle at the front of a robot indicates its heading. The arrows represent the interactions between robots. Arrow direction indicates the identity (color) of the robot that exerts its influence on the robot to which the arrow points. The small dots in front of the robots represent the next target places.

S11 Video. Swarm robotics experiment where robots interact with $k = 2$ neighbors selected randomly. Top: Typical experiment with a group of 5 robots in a circular arena of radius 420 mm, captured by the top camera. The border of the arena is represented by the red circle. Purple circles represent the individual robot safety area, of diameter 8 cm. Small green dots in front of robots indicate their next target place. The video is accelerated 6 times. Total duration: 6 minutes. Bottom: Relative movement of the robots with respect to the barycenter of the group. The barycenter is represented by the black disk and remains oriented to the right. Robots are represented by colored disks with their identification number in the center. The small circle at the front of a robot indicates its heading. The arrows represent the interactions between robots. Arrow direction indicates the identity (color) of the robot that exerts its influence on the robot to which the arrow points. The small dots in front of the robots represent the next target places.

S12 Video. Swarm robotics experiment where robots interact with the $k = 3$ nearest neighbors. Top: Typical experiment with a group of 5 robots in a circular arena of radius 420 mm, captured by the top camera. The border of the arena is represented by the red circle. Purple circles represent the individual robot safety area, of diameter 8 cm. Small green dots in front of robots indicate their next target place. The video is accelerated 6 times. Total duration: 6 minutes. Bottom: Relative movement of the robots with respect to the barycenter of the group. The barycenter is represented by the black disk and remains oriented to the right. Robots are represented by colored disks with their identification number in the center. The small circle at the front of a robot indicates its heading. The arrows represent the interactions between robots. Arrow direction indicates the identity (color) of the robot that exerts its influence on the robot to which the arrow points. The small dots in front of the robots represent the next target places.

S13 Video. Swarm robotics experiment where robots interact with $k = 3$ neighbors selected randomly. Top: Typical experiment with a group of 5 robots in a circular arena of radius 420 mm, captured by the top camera. The border of the arena is represented by the red circle. Purple circles represent the individual robot safety area, of diameter 8 cm. Small green dots in front of robots indicate their next target place. The video is accelerated 6 times. Total duration: 6 minutes. Bottom: Relative movement of the robots with respect to the barycenter of the group. The barycenter is represented by the black disk and remains oriented to the right. Robots are represented by colored disks with their identification number in the center. The small circle at the front of a robot indicates its heading. The arrows represent the interactions between robots. Arrow direction indicates the identity (color) of the robot that exerts its influence on the robot to which the arrow points. The small dots in front of the robots represent the next target places.

S14 Video. Swarm robotics experiment where robots interact with every other robot ($k = 4$). Top: Typical experiment with a group of 5 robots in a circular arena of radius 420 mm, captured by the top camera. The border of the arena is represented by the red circle. Purple circles represent the individual robot safety area, of diameter 8 cm. Small green dots in front of robots indicate their next target place. The video is accelerated 6 times. Total duration: 6 minutes. Bottom: Relative movement of the robots with respect to the barycenter of the group. The barycenter is represented by the black disk and remains oriented to the right. Robots are represented by colored disks with their identification number in the center. The small circle at the front of a robot indicates its heading. The arrows represent the interactions between robots.

Arrow direction indicates the identity (color) of the robot that exerts its influence on the robot to which the arrow points. The small dots in front of the robots represent the next target places.

S1 Fig. Density map of cohesion and polarization for fish and model simulations, normalized with the number of data per range of polarization. Density map of cohesion for different ranges of the polarization, for fish and for the 11 strategies used in the model simulations. Units of cohesion is cm in fish and λ_{M} cm in simulations ($\lambda_{\mathrm{M}} = 0.87$). Color intensity is number of data in boxes normalized with the total number of data in the grid ($\times 1000$). We used 40×50 boxes.

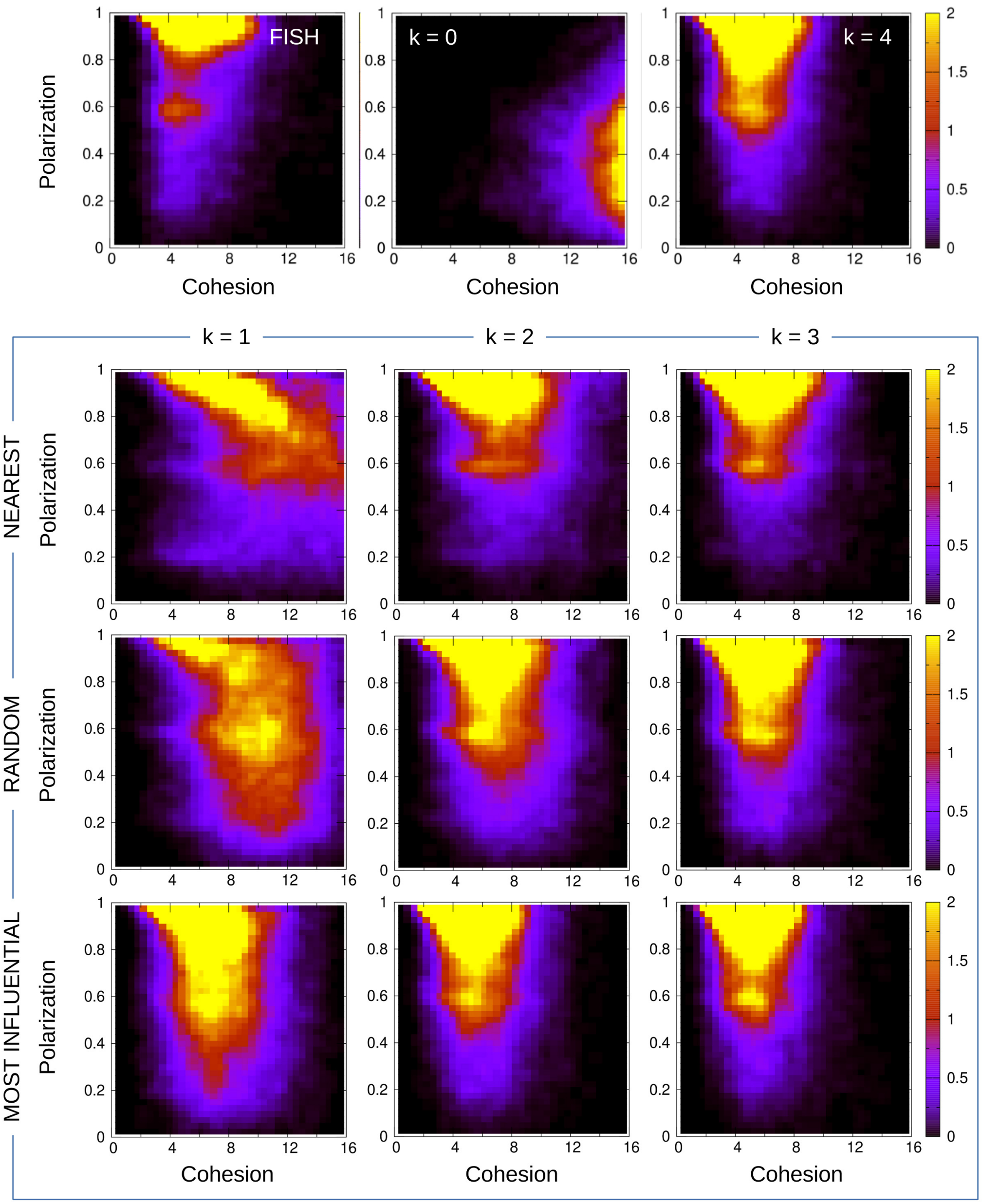

S2 Fig. Density map of cohesion and polarization for fish and robotic swarm, normalized with the total number of data.
Density map of cohesion for different ranges of the polarization, for fish and for the 10 strategies implemented in the robotic swarm. Units of cohesion is cm in fish and λ_{R} cm in robots ($\lambda_{\mathrm{R}} = 0.35$). Color intensity is number of data in boxes normalized with the total number of data in the grid ($\times 1000$). We used 40×50 boxes.

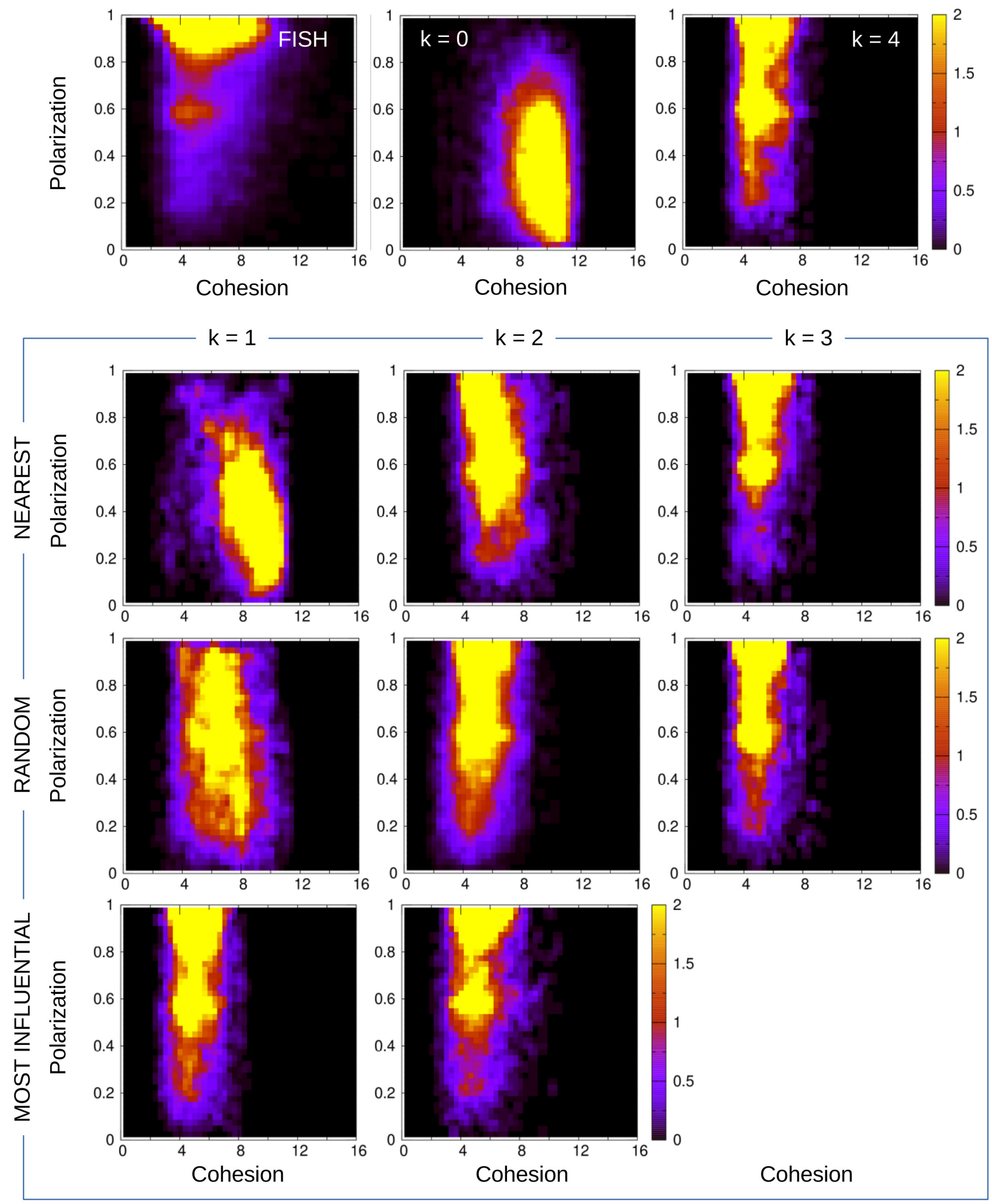

S3 Fig. Density map of cohesion and polarization for fish and model simulations, normalized with the number of data per range of polarization. Density map of cohesion for different ranges of polarization, for fish and for the 11 strategies used in the model simulations. Units of cohesion is cm in fish and λ_{M} cm in simulations. Color intensity is number of data in boxes normalized with the number of data per interval of polarization, *i.e.*, each row is the PDF of the cohesion for a range of values of the polarization. We used 40×50 boxes.

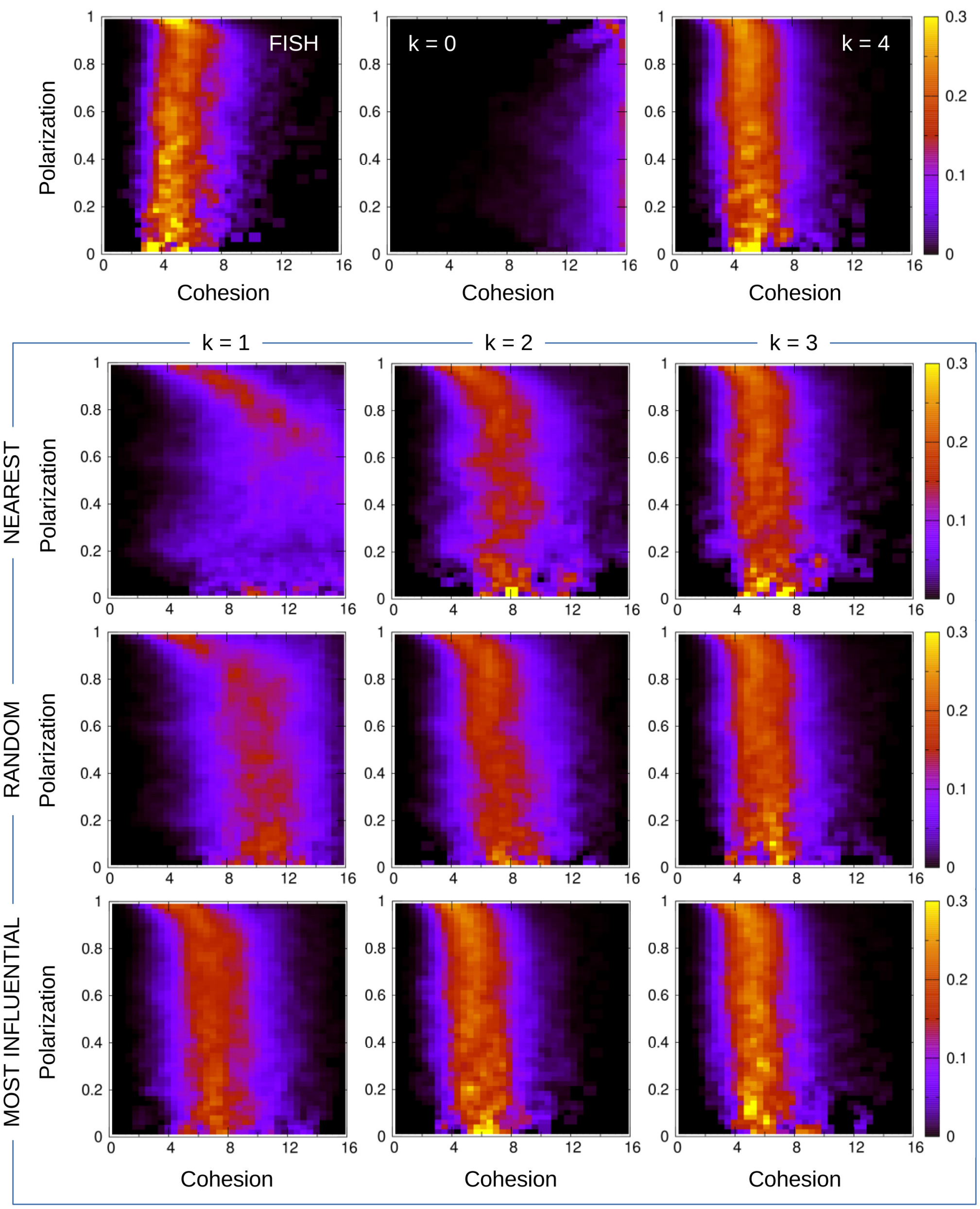

S4 Fig. Density map of cohesion and polarization for fish and robotic swarm, normalized with the total number of data.
Density map of cohesion for different ranges of polarization, for fish and for the 10 strategies used in the robotic swarm. Units of cohesion is cm in fish and λ_{M} cm in simulations. Color intensity is number of data in boxes normalized with the number of data per interval of polarization, *i.e.*, each row is the PDF of the cohesion for a range of values of the polarization. We used 40×50 boxes.

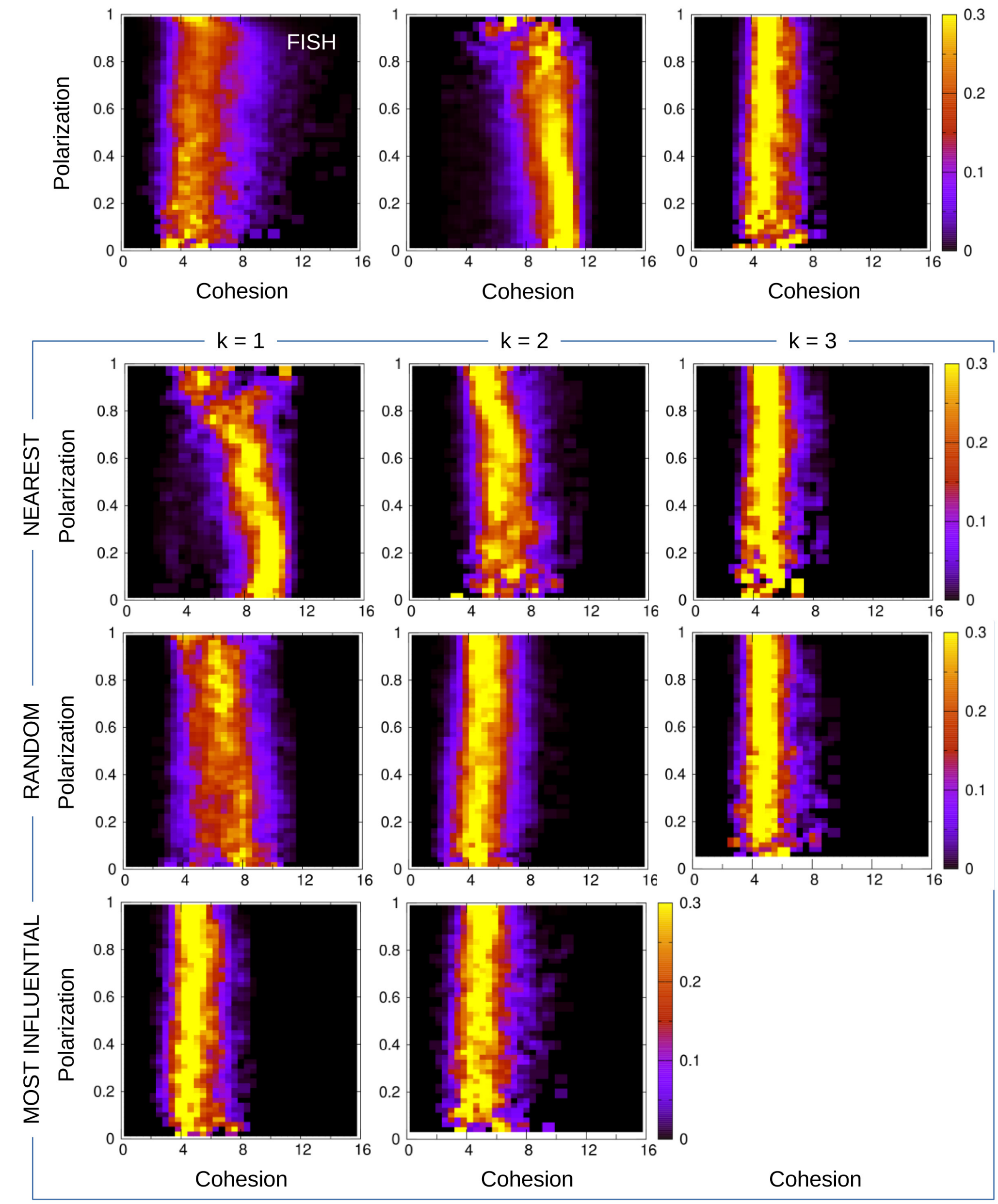

S5 Fig. Counter-milling in model simulations. Red arrows denote velocity field (mean speed and direction) of agents in the reference system of the barycenter of the group, here located at coordinates $(0, 0)$. Orange circle denotes the average relative position of the border of the arena with respect to the barycenter. The cases where agents interact with the $k = 3$ most influential neighbors (statistically identical to the case where $k = 4$) and where agents do not interact ($k = 0$) are not depicted.

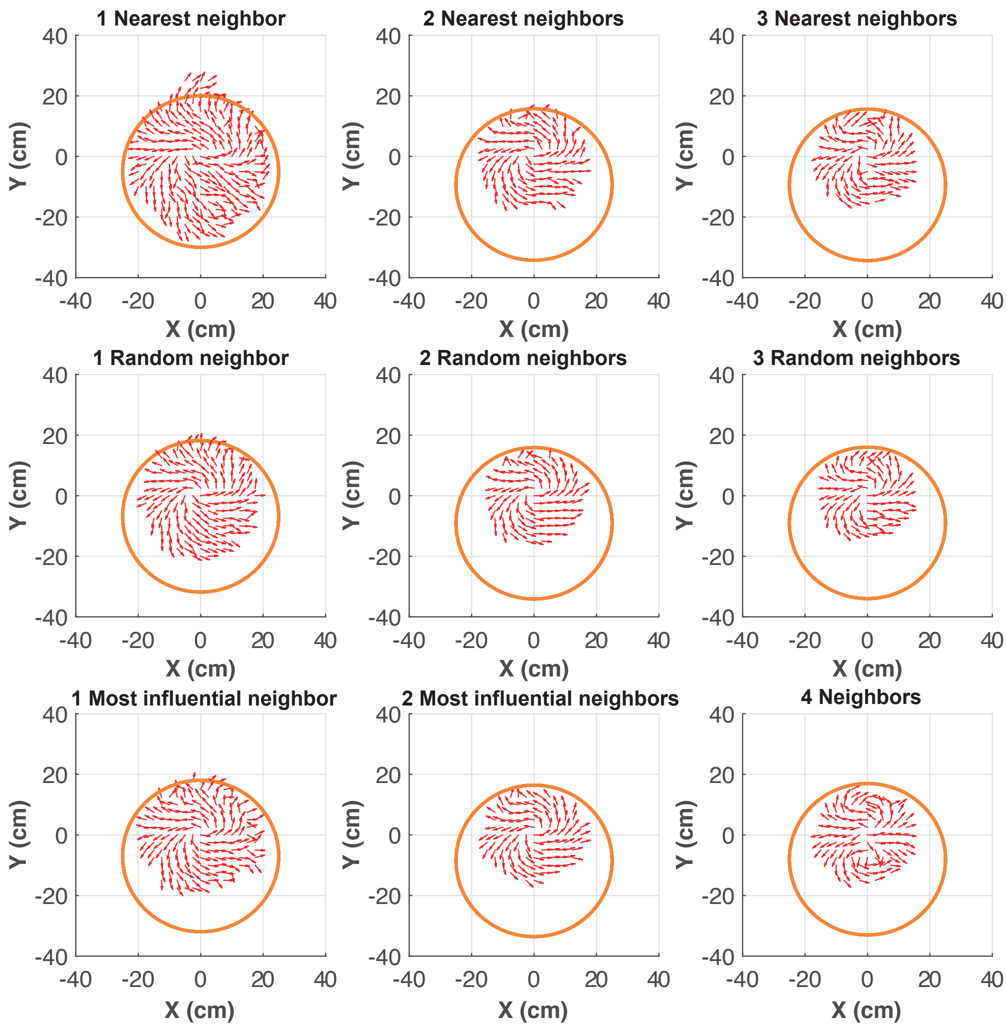

S6 Fig. Counter-milling in robotics swarm experiments. Red arrows denote velocity field (mean speed and direction) of robots in the reference system of the barycenter of the group, here located at coordinates $(0, 0)$. Orange circle denotes the average relative position of the border of the arena with respect to the barycenter. The cases where robots interact with the $k = 3$ most influential neighbors (statistically identical to the case where $k = 4$) and where robots do not interact ($k = 0$) are not depicted.

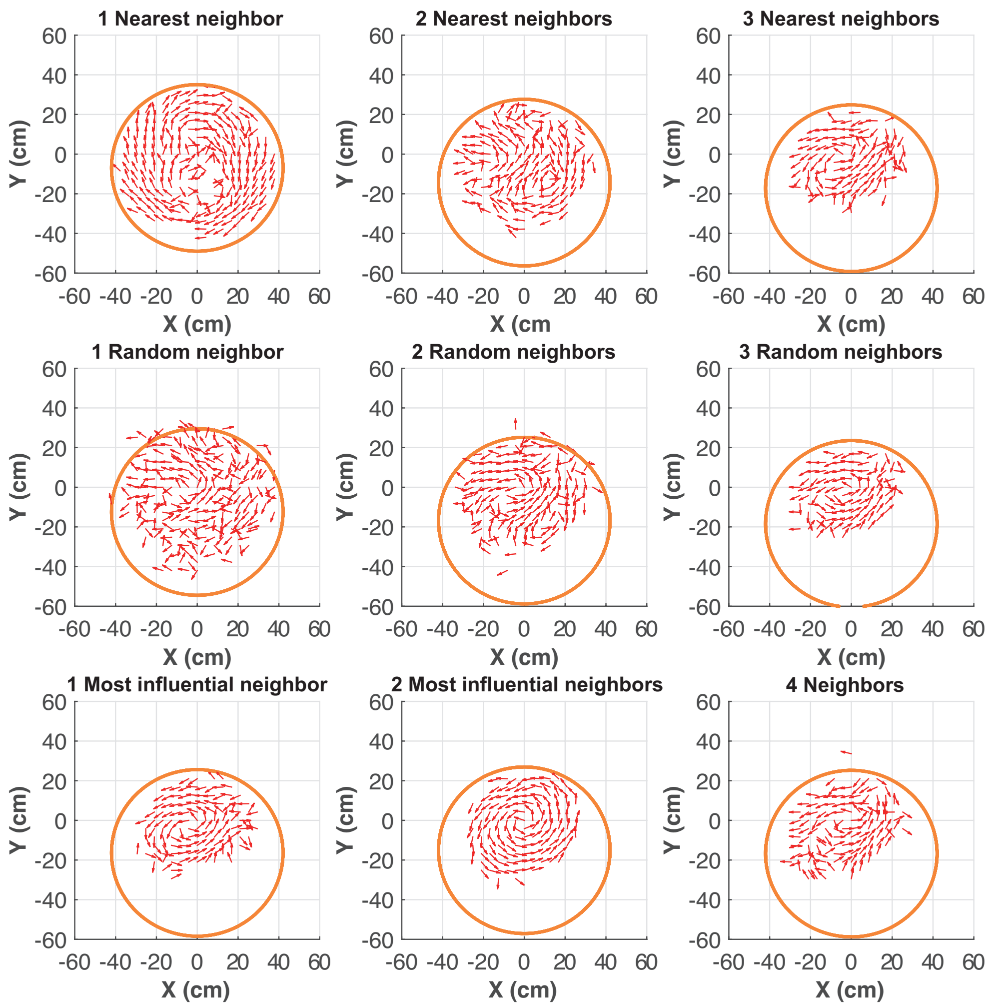

S7 Fig. Interaction functions with the wall and between individuals, extracted from experiments of fish swimming in pairs [14]. (A) Intensity of the repulsion from the wall $f_{\mathrm{w}}(r_{\mathrm{w},i})$ (green) as a function of the distance to the wall $r_{\mathrm{w},i}$, and intensity of the attraction $f_{\mathrm{Att}}(d_{ij})$ (red) and the alignment $f_{\mathrm{Ali}}(d_{ij})$ (blue) between fish i and j as functions of the distance d_{ij} separating them. (B) Normalized odd angular function $O_{\mathrm{w}}(\theta_{\mathrm{w},i})$ modulating the interaction with the wall as a function of the relative angle to the wall $\theta_{\mathrm{w},i}$. (C) Normalized angular functions $O_{\mathrm{Att}}(\psi_{ij})$ (odd, in red) and $E_{\mathrm{Att}}(\phi_{ij})$ (even, in orange) of the attraction interaction, and (D) $O_{\mathrm{Ali}}(\phi_{ij})$ (odd, in blue) and $E_{\mathrm{Ali}}(\psi_{ij})$ (even, in violet) of the alignment interaction between agents i and j, as functions of the angle of perception ψ_{ij} and the relative heading ϕ_{ij}.

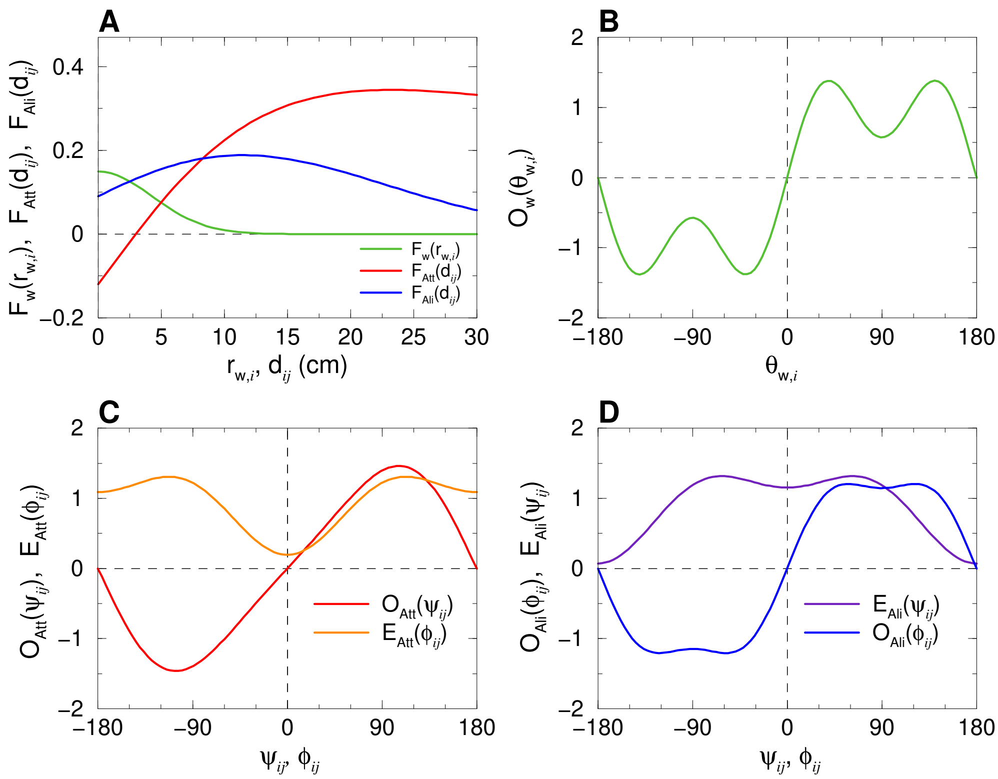

Parameter	**Symbol**	**Model**	**Robots**
Intensity of heading random fluctuations	γ_{R}	0.45	0.1
Fluctuations reduction factor when close to wall	α	0.67	1
Intensity of wall repulsion	γ_{w}	0.15	0.79
Range of wall repulsion (cm)	l_{w}	6	11
Intensity of attraction/repulsion	γ_{Att}	0.12	0.18
Range of attraction between individuals (cm)	l_{Att}	20	37
Distance of balance of attraction/repulsion (cm)	d_{Att}	3	18
Intensity of alignment	γ_{Ali}	0.09	0.04
Range of alignment between individuals (cm)	l_{Ali}	20	37
Distance of alignment (cm)	d_{Ali}	6	5
Average duration between successive kicks (s)	τ	0.5	1.3
Mean length between two successive kicks (cm)	l	7	7.4
Typical individual velocity in active period (cm/s)	v_0	14	3.75
Relaxation time (s)	τ_0	0.8	0.9

Table 1. Values and units of the parameters for model simulations and robots.